RESEARCH ARTICLE | OCTOBER 02 2023

Understanding and modeling unstarting phenomena in a supersonic inlet cascade

Special Collection: Shock Waves

Noraiz Mushtaq ; Paolo Gaetani

Physics of Fluids 35, 106101 (2023)
https://doi.org/10.1063/5.0160706

Physics of Fluids ARTICLE pubs.aip.org/aip/pof

Understanding and modeling unstarting phenomena in a supersonic inlet cascade

Cite as: Phys. Fluids **35**, 106101 (2023); doi: 10.1063/5.0160706
Submitted: 5 June 2023 · Accepted: 7 September 2023 ·
Published Online: 2 October 2023

Noraiz Mushtaq and Paolo Gaetani[a)]

AFFILIATIONS

Laboratory of Fluid Machines (LFM), Department of Energy, Politecnico di Milano, Via Lambruschini 4, 20156 Milan, Italy

Note: This paper is part of the special topic, Shock Waves.
[a)]**Author to whom correspondence should be addressed:** paolo.gaetani@polimi.it

ABSTRACT

The renewed interest in supersonic turbomachinery research was driven by its potential applications in emerging fields. However, the design of supersonic inlet cascades faces significant challenges due to the inherent limitations of supersonic flows. While several studies have been published on the unstarting of supersonic intakes, there exists a major knowledge gap in the unstarting of supersonic blade rows. This paper presents the research on a novel unstarting mechanism for supersonic inlet cascades induced by the formation of a collective shock. Tailored simulations were carried out to study the coalescence of the leading-edge bow shock waves and to investigate the stability and the hysteresis of this phenomenon. Then, a reduced order model was developed and verified to estimate the limit induced by this additional unstarting mechanism. Since the accuracy of the unstarting condition relies heavily on the predicted bow shock shape, novel strategies were proposed to improve the estimate of the asymptotic slope of the bow shock and to account for large incidence angles. Furthermore, the well-known Kantrowitz criterion for the self-starting of a supersonic channel was reviewed and adapted to supersonic blade rows by considering both weak and strong oblique shock waves in the calculation of the maximum contract ratio. Then, it was demonstrated the importance of accounting for shock-induced boundary layer separation in the starting process of a supersonic machine. Finally, computational fluid dynamics simulations reveal the high sensitivity of the self-starting limit to the cascade solidity and profile shape.

I. INTRODUCTION

Supersonic turbines are typically light and compact machines that provide large specific work outputs at the expense of lower efficiencies compared to their subsonic counterpart.[1] Thanks to their characteristics, their application spans over a variety of fields: power production, aircraft engines, rocket engines, and marine propulsion.

The earliest instances of supersonic turbomachinery can be traced back to steam turbines,[2] in which the high-pressure supersonic impulse stage reduced the thermal burden on the subsequent stages by lowering the total inlet temperatures.[3–7] From the second half of the twentieth century, supersonic turbines have become the standard solution to power rocket fuel pumps because of their large work-to-weight ratio;[8–10] furthermore, the design of the low-pressure stages of steam turbines also required supersonic profiles at the tip section.[11,12]

Over the past decade, there has been a renewed focus on supersonic turbomachinery research, driven by the demand for its application in two emerging areas: rotating detonation engines (RDEs) and organic Rankine cycles (ORCs).

In an RDE, the combustion process is carried out by a detonation wave that rotates in an annular channel (other geometries are also viable) and burns the fresh mixture.[13] The pressure gain generated by the detonation wave provides several benefits, including reduced fuel consumption,[14,15] higher total pressure[16] (up to 15%), and increased thermal and plant efficiency[17] (up to 14% more than traditional solutions for intermediate pressure ratios[18]). The rotating detonation combustor (RDC) delivers a supersonic and highly fluctuating flow, which renders the adoption of a supersonic inlet turbine particularly suited for this application. Design and optimization of a supersonic inlet turbine for RDEs have been presented in the works by Paniagua *et al.*[19–21] and Mushtaq *et al.*[22,23] Supersonic turbine interaction with the RDC has been investigated numerically by Sousa *et al.*,[24] Braun *et al.*,[25] Shen *et al.*,[26] and Su *et al.*[27] and experimentally by Bach *et al.*[28] The development of an aerodynamically efficient supersonic inlet turbine becomes even more complex due to the cooling demands necessary to withstand the extremely high flow temperatures from the rotating detonation combustor. To address this challenge, Lozano and Paniagua[29] suggested implementing leading-edge cooling injection to alleviate thermal loading;

concurrently, ongoing investigations are exploring the use of C/SiC composites for their potential in moderating the cooling requirements for pressure gain combustion systems.[30] Moreover, an insightful study by Stathopoulos[31] quantified the impact of turbine cooling on the efficiency of a Humphrey cycle with pressure gain combustion.

On the other hand, organic Rankine cycles represent an efficient way to extract power from energy sources characterized by low-to-medium temperature levels.[32] Because of the high expansion ratio and low speed of sound (organic fluids), ORC turbines typically consist of only a few supersonic or transonic blade rows.[33] Bufi and Cinnella[34] developed a preliminary design methodology for dense-gas supersonic axial turbines, while Colonna *et al.*[35] and Romei *et al.*[36] studied the real-gas effects in the nozzle of a supersonic cascade.

Designing a supersonic turbine requires careful consideration of the additional complexities introduced by supersonic flows. The primary concern is limiting shock losses, which account for the majority of the entropy production in these machines.[22,37] However, achieving high-efficiency operating conditions is challenging due to the characteristic constraints of supersonic flows; if the axial Mach number is subsonic, the mass flow is restricted by the unique incidence relation between the inlet Mach number and the inlet flow angle.[38] Furthermore, adequate safety margins should be included to prevent unstarting in design as well as in off-design conditions. Lichtfuss and Starken[39] provided a comprehensive report of the challenges posed by supersonic turbomachinery with in-depth description of the various supersonic flow regimes encountered at the inlet and outlet of supersonic cascades.

The starting of a supersonic channel is the process of accelerating a flow from subsonic to supersonic conditions.[40] A channel is considered self-starting when it is able to ingest the shock structures generated during the starting process without any geometry variation. Once the channel is started, weak oblique shock structures and a supersonic flow are observed from inlet to outlet; in contrast, an unstarted channel is identified by strong shock structures at the inlet section, which result in a transition to a subsonic flow. Kantrowitz and Donaldson[41] presented the pioneering work of this field introducing the concept of unstarting and calculating the maximum contraction ratio for a started supersonic diffuser. Since then, a considerable amount of literature has been published on the unstart of supersonic/hypersonic inlets and several unstaring mechanisms have been identified: Unstarting can be triggered by the contraction ratio, backpressure, fuel addition, heat release, and Mach number.[42]

Meanwhile, there still exists a critical gap in the study of unstarting phenomena in supersonic cascades. While Kantrowitz attempted to address this gap by applying his one-dimensional and inviscid theory developed for supersonic diffusers to supersonic cascades,[43] he acknowledged that his hypothesis was "more than a speculation and much more work will have to be done before the starting mechanism is fully understood." However, no new research has been published on the subject in the last seventy years, and the Kantrowitz theory continues to be the accepted method for evaluating starting in supersonic cascades.[19,22,34] Considering the renewed interest in supersonic turbines for their potential application in RDEs and ORCs, further research is urgently needed to improve our understanding of the complex flow dynamics occurring during the starting and unstarting of supersonic cascades. Furthermore, accurate identification of the unstarting limit will be particularly beneficial for supersonic inlet turbines, since these machines exhibit their highest efficiency close to the Kantrowitz limit.[23]

The structure of this work is as follows: Section II describes the fundamental methodologies applied throughout the study; in particular, Sec. II B contains all the details of the computational flow model with the grid independence analysis and the solver validation for supersonic applications. Section III presents a novel unstarting phenomenon for supersonic inlet cascades induced by the formation of a collective shock. The unstarting mechanism is described in Sec. III A 1, while the stability and hysteresis of collective shocks inside the inlet channel are investigated in Sec. III A 2. Furthermore, a reduced order model (ROM) to predict the formation of the collective shock is developed (Sec. III B). Given that the accuracy of the predicted unstarting condition heavily relies on the shape of the bow shock waves, Secs. III B 1 and III B 2 propose novel strategies to improve the estimate of the final slope of the bow shock and to account for large incidence angles. Then, the unstarting limit curves predicted by the model are verified against accurate computational fluid dynamics (CFD) simulations (Sec. III B 3). Finally, Sec. IV extends Kantrowitz's original theory to supersonic cascades and examines the effect of the shock-induced boundary layer separation on the calculation of the self-starting Mach number.

II. RESEARCH METHODS

A. Method of characteristics for supersonic profile generation

The vortex-flow method, an implicit method of characteristics (MOC) developed by Goldman and Vanco,[44] was employed for the generation of the supersonic profiles. In this methodology, a supersonic uniform flow at the inlet is converted into a free vortex-flow (the product of the velocity and the radius of curvature of the streamline is constant) by the inlet transition arcs; then, the vortex-flow is turned by the circular arcs and finally, the outlet transition arcs re-transform it back into a uniform flow. This design strategy was preferred over other solutions available in the literature[39] since it guarantees a smooth velocity distribution with the highest loading at mid-chord.

The resulting profile from the vortex-flow method has zero thickness at the leading and trailing edges. Hence, the pressure surface and the suction surface are shifted by a reasonable thickness value and closed with ellipses; a high semi-axis ratio was selected for the ellipses because they have been proven to be more efficient in supersonic cascades.[23]

The performance of a supersonic profile is highly dependent on two dimensionless ratios: the chord over pitch ratio c/g (solidity) and the leading-edge thickness over pitch ratio th/g [Figs. 1(a) and 1(b)]. Typically, these values are selected to achieve maximum efficiency, while satisfying mechanical constraints and cooling requirements. However, the objective of this study is not to design the most efficient supersonic turbine for a specific application, but rather to investigate unstarting phenomena. Therefore, the dimensionless ratios, the stream tube channel height ratio, and the flow quantities were carefully selected to isolate Kantrowitz unstarting from collective shock unstarting.

B. Computational flow model

1. Numerical methods and boundary conditions

Quasi-3D computational fluid dynamic (CFD) simulations were performed to describe the flow behavior in the blade-to-blade plane.

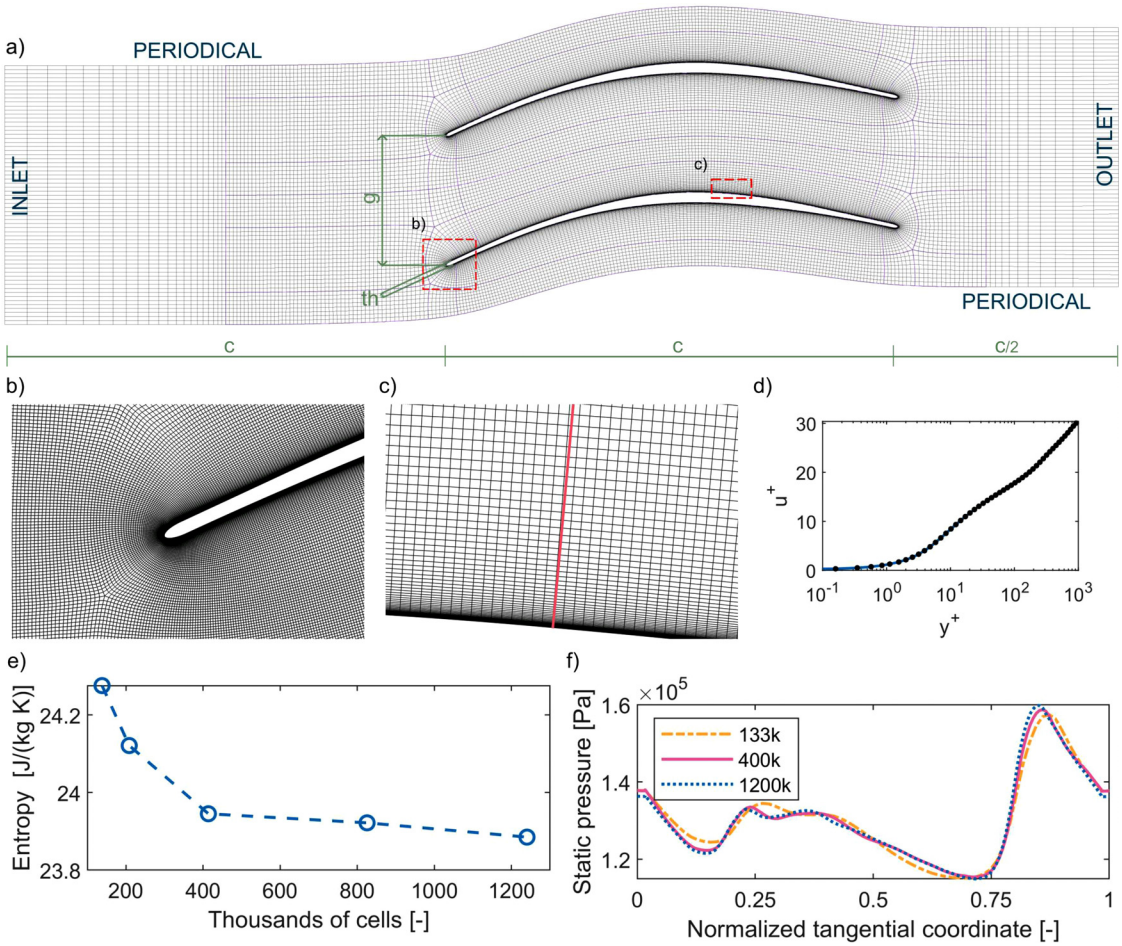

FIG. 1. (a) Overview of the computational domain with boundary conditions. The HOH topology of the mesh is displayed through a very coarse mesh (40k). (b) and (c) Details of the 400k-cell mesh around the leading edge and in the boundary layer. (d) Velocity profile extracted along the line displayed in c for the 400k-cell mesh. (e) Grid convergence analysis on the mass-flow averaged entropy production from inlet to outlet. (f) Static pressure distribution along the tangential direction extracted on the outlet plane.

Computations were carried out on ANSYS CFX (Release 21.1),[45] which is implemented as an element-based finite volume method with a pressure-based implicit coupled solver. The advection terms were discretized by the total variation diminishing (TVD) high-resolution algorithm;[46] the scheme employs a nonlinear recipe for the blending factor[45] based on the boundedness principles of Barth and Jespersen.[47] The transient terms were discretized by a second-order backward Euler scheme.

Viscous calculations were required by the possibility of boundary layer separation at large incidence angles and by the shock-wave/boundary-layer interaction. Turbulence closure for the Reynolds-averaged Navier–Stokes (RANS) equations was achieved through the k-omega shear stress transport (SST) model, while y^+ was maintained below 1 for proper boundary layer resolution [Figs. 1(c) and 1(d)]. At the current stage of the problem analysis, the impact of turbulence intensity (TI = 5%) and eddy viscosity ratio ($\mu_t/\mu = 10$) was deemed to be of secondary importance.

Static pressure, temperature, and velocity were all assigned at the supersonic inlet. Adiabatic and no-slip conditions were selected for the blade walls, while adiabatic and free-slip conditions were prescribed for the hub and shroud walls. The outlet was defined as supersonic, and periodic conditions were applied on the lateral boundaries to properly simulate a single blade channel. The working fluid is air, modeled as a perfect gas. Finally, calculations were considered at convergence when the residuals were below 5×10^{-6} at each time step or the last step in a steady-state simulation.

2. Domain definition and mesh generation

The domain for the quasi-3D simulation was modeled as a periodic annular stream tube with a small thickness in the radial direction and placed at a large radius to minimize curvature and radial equilibrium effects. The inlet is located a chord upstream of the leading edge, while the outlet is situated half-chord downstream of the trailing edge [Fig. 1(a)].

Ansys TurboGrid (Release 21.1)[48] was utilized to produce a high orthogonality and low skewness block-structured mesh composed of hexahedral cells. To ensure grid independence, meshes of different

sizes were examined, and the converging trend for mass-flow averaged entropy production is presented in Fig. 1(e). Grid independence was quantitatively evaluated with the grid convergence index (GCI) methodology by Celik *et al.*:[49] The GCI from medium to refined mesh (200k, 400k, and 800k) calculated on the entropy production is 0.07%. Furthermore, Fig. 1(f) reveals a negligible difference in the static pressure distribution (extracted on the outlet section) between the 400k mesh and the 1200k one. Based on these results, the 400k-cell mesh was selected for all the simulations.

3. Solver validation

ANSYS CFX solver was validated for supersonic applications against four test cases. Each test case involved proper domain definition, assignment of correct boundary conditions, and a grid independence analysis. Although a detailed discussion of each problem is omitted for the sake of brevity and lack of novelty, the results are presented to fulfill the purpose of solver validation.

In the Sod shock tube problem,[50] the rupture of a diaphragm produces a shock wave, a contact surface, and an expansion wave propagating in the domain at different speeds. Figure 2 showcases solver proficiency in predicting strength, position, and speed of all three features.

The second test case is the inviscid supersonic wedge, which creates an oblique shock in a supersonic flow. Eight different conditions were tested (two wedge angles θ at four inlet Mach numbers) and the solver precisely estimated the slope of the oblique shock waves (Fig. 3).

The shock-wave/boundary layer interaction problem, investigated experimentally by Settles and Dodson[51,53] on a 2D compression corner, combines turbulence, compressibility, and viscous-inviscid

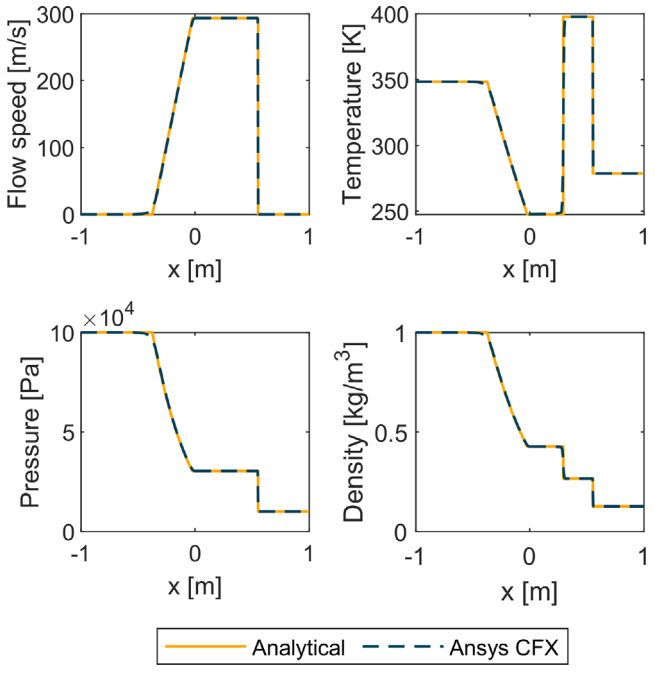

FIG. 2. Comparison between the analytical and ANSYS CFX solution at t = 0.001 s for the Sod shock.

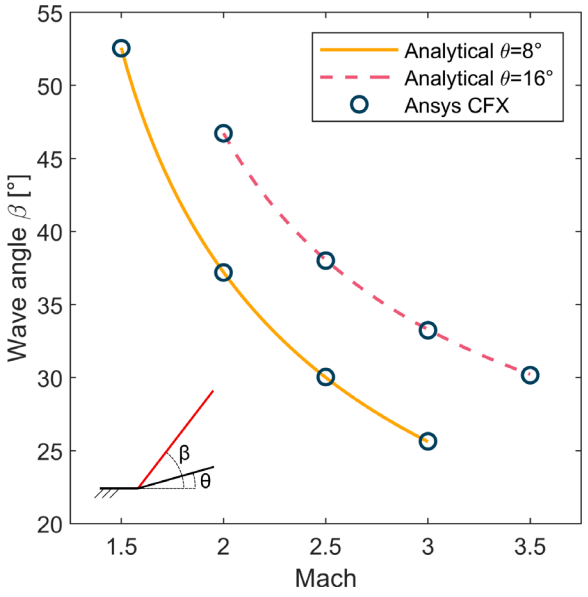

FIG. 3. Comparison between ANSYS CFX and the analytical solution for the inviscid supersonic wedge problem.

interaction phenomena. 8° and 16° corner ramp angles were simulated, and CFX reproduces accurately the starting point of pressure increase, the maximum pressure after the shock, and the overall trend of the pressure on the wall (Fig. 4).

Finally, at the Laboratory of Compressible fluid dynamics for Renewable Energy Applications (CREA Lab) at Politecnico di Milano, a total pressure probe was inserted in the Test Rig for Organic Vapors (TROVA).[52] The N2 flow, accelerated up to Mach 1.7 through a

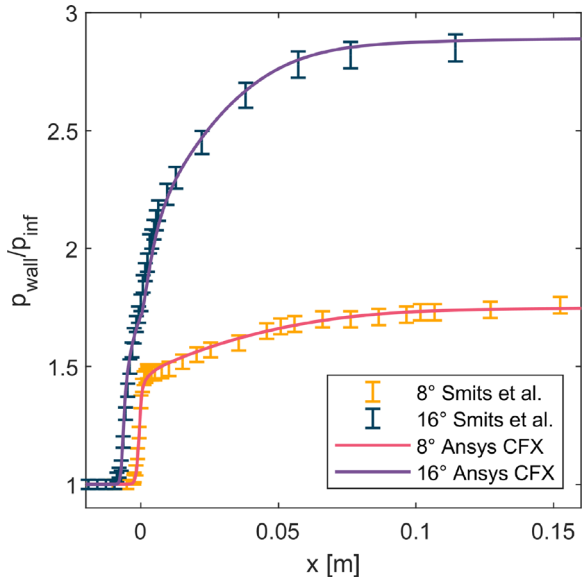

FIG. 4. Comparison between the experimental data[51] and ANSYS CFX for the compression corner problem at 8° and 16° ramp angles.

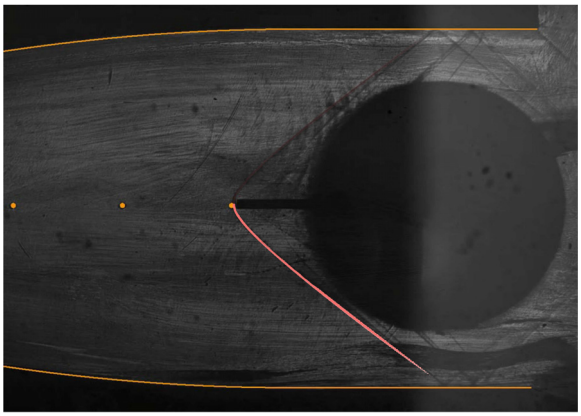

FIG. 5. Comparison between the experimental activity at the CREA lab[52] and ANSYS CFX for the bow shock shape prediction. The schlieren image is displayed in background, while the bow shock extracted from CFD is shown in foreground (the top half is transparent for the comparison). Adapted from Conti *et al.*, Exp. Fluids **63**, 117 (2022). Copyright 2022 Author(s), licensed under a Creative Common Attribution (CC BY) license.

converging–diverging nozzle, impinged on the probe tip and generated a bow shock wave. The bow shock shape post-processed from the CFD simulation (in the foreground) presents excellent agreement with the Schlieren image of the experimental activity (in the background) (Fig. 5).

Each of the above test cases was carefully selected because all these features of supersonic flows will play a crucial role in the study of unstarting phenomena in supersonic turbines.

III. COLLECTIVE SHOCK UNSTARTING

A. Description of the unstarting mechanism

1. The formation of a collective shock

The problem of proximal bodies in supersonic flows is encountered in many applications,[55] such as launch vehicle stage separation, binary asteroid systems entering the planetary atmosphere, or a dust cloud.[54] A collective bow shock is formed ahead of two binary bodies when the distance between their centers is reduced and the two separate bow shock waves merge. Boiko observed this phenomenon experimentally in shock tube tests[54] and identified three distinct stages of the transition (Fig. 6): In the first stage (a), each body generates a separate bow shock wave with a regular intersection; as the distance between the bodies is decreased or the Mach number reduced (b), the intersection generates a Mach phenomenon, which is recognized by its typical structure composed of a normal shock between the two triple points;[56] and finally (c), a collective bow shock wave is generated for low distances or low Mach numbers.

The leading edge of a supersonic profile generates a bow shock; hence, supersonic turbines resemble the problem of proximal bodies in supersonic flows. If the geometry of the machine is fixed (pitch and leading edge) and the inlet Mach number is progressively reduced, the bow-shock waves widen and gradually transform from a regular intersection to a collective shock wave.

However, there is a relevant difference between the two cases: The collective shock wave formed in a supersonic turbine is confined

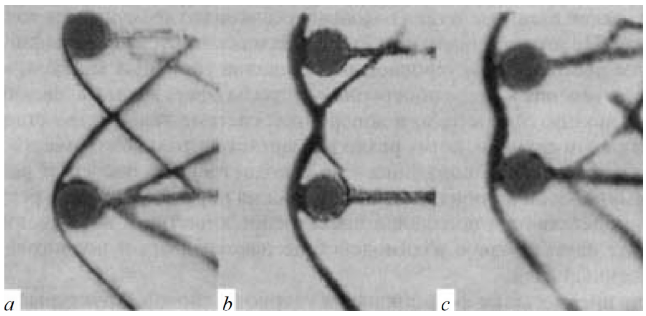

FIG. 6. (a) Schlieren photographs of the types of bow shock interference ahead of a transverse system of spheres (From Boiko[54]). Reproduced with permission from Laurence *et al.*, Fluid Dyn. **39**, 330–338 (2004). Copyright 2004 Springer Nature.

by the channel walls with further consequences related to the starting/unstarting dynamics. Moreover, the periodicity of a turbine blade row can be interpreted as an infinite number of bodies, which explains the absence of the oblique portion of the bow-shock wave and why the collective shock of a supersonic turbine is straight and normal to the channel axis (Fig. 7).

Considering the orientation of the flow, which is not necessarily aligned with the channel axis, the collective shock wave can be classified as either a weak or strong oblique shock wave in function of the inlet Mach number and the wave angle β (Fig. 8). The formation of a collective shock for a large inlet flow angle α occurs at high inlet Mach numbers. In these conditions, the combination of a small wave angle β with a large Mach number is consistent with a weak solution of the oblique shock wave [Fig. 8(a)]. On the contrary, for smaller flow angles α, the two bow shock waves merge at lower inlet Mach numbers. The collective shock generated in these conditions behaves as a strong oblique shock wave, a solution that is compatible with large wave angles β and small Mach numbers [Fig. 8(b)]. As known from the classical theory of aerodynamics,[57] the flow is turned by an angle θ across an oblique shock wave and it is, respectively, supersonic or subsonic for a weak or strong solution (except for a small region near θ_{max}).

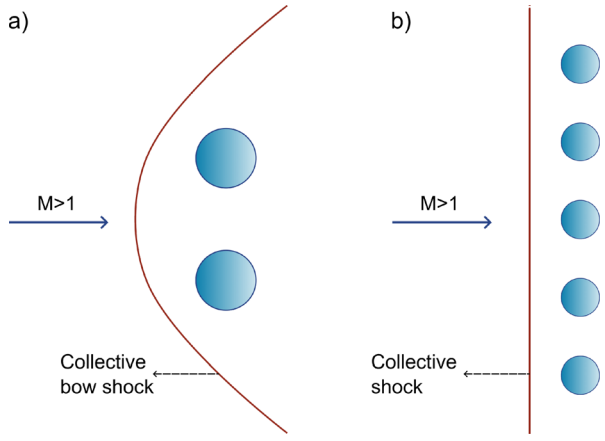

FIG. 7. In the binary sphere problem (a), the collective shock has a bow-shape, whereas in the case of a supersonic turbine (b), the shock wave is straight and orthogonal to the channel axis (infinite spheres due to periodical conditions).

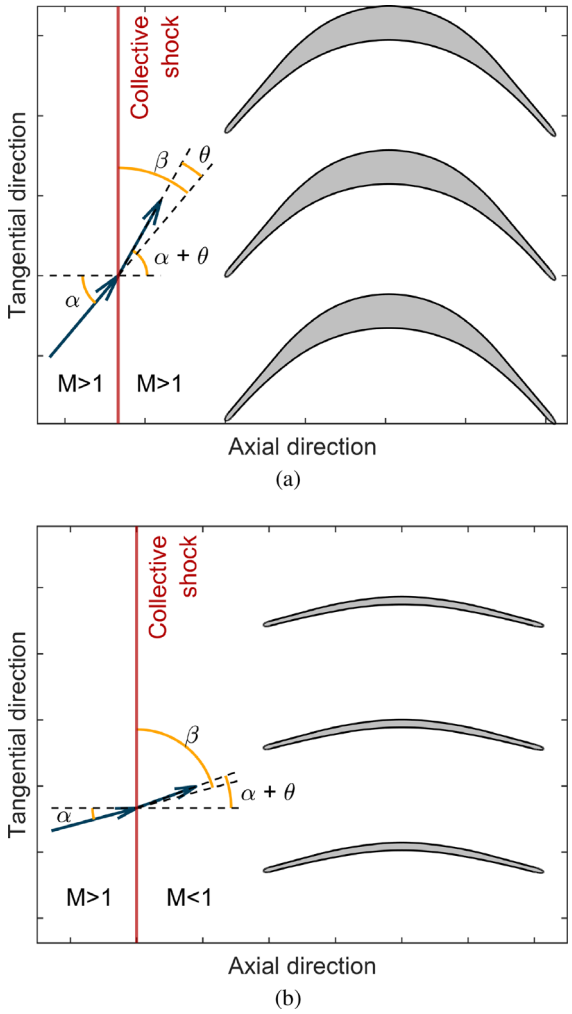

FIG. 8. Collective shock as a weak oblique shock wave for high inlet Mach number and high flow angle (a) and as a strong oblique shock wave for low inlet Mach number and low flow angle (b).

The mechanism behind the formation of a collective shock has been thus far outlined through several sketches. However, to confirm this theory, it is necessary to perform an unsteady CFD simulation on a representative case. The geometry adopted for this purpose has an inlet geometric angle of 25° and an outlet geometric angle of 12.5° (half of the inlet geometric angle), with a blade height ratio of 1.2 and a pitch to leading-edge thickness ratio of 42. These specific values were selected to avoid Kantrowitz unstarting in all tested conditions. The inlet Mach number was gradually reduced from 1.70 to 1.375. (The corresponding axial inlet Mach numbers are 1.54 and 1.25.) The length of each step ($\Delta t = 0.025$ s) is five times the time taken by the left running characteristic (V_z–C) to travel from the inlet to outlet of the domain [Fig. 9(a)]. It is relevant to underline that this article describes the formation of a collective shock in a supersonic turbine only from a quasi-steady perspective, which means that the inlet conditions are varied slowly enough (or sufficient time is provided after each variation) to achieve a quasi-steady behavior; the effect of unsteady inlet conditions with variable frequency, amplitude, and mean value on collective shock generation was investigated by Mushtaq and Gaetani in a dedicated work.[58]

Starting from an inlet Mach number of 1.7, the leading edges generate two distinct bow shock waves with a regular intersection [Fig. 9(b)]. As the inlet Mach number is progressively reduced, the bow shock waves widen and open up. At a certain condition, the bow shock waves partially merge at the intersection point, producing the characteristic structure of a Mach phenomenon[56] [Fig. 9(c)]. Further reduction of the inlet Mach number increases the area of merger between the bow shock waves, causing one of the legs of the Mach reflection to disappear. This leads to the formation of a new structure, namely, a lambda shock [Fig. 9(d)]. Finally, as the inlet Mach number is further decreased, the two bow shock waves merge completely, resulting in the formation of a collective shock with the same characteristics described previously [Fig. 9(e)]: The collective shock is straight and normal to the channel axis; in addition, the collective shock is a strong oblique shock wave, which is consistent with the low inlet geometric angle of the blade. Since the Mach number behind the strong shock is subsonic but close to unity in this case, the leading-edge contraction is sufficient for the transition to supersonic Mach numbers.

The intersection between the bow shock waves is the necessary condition for the formation of a collective shock, but for certain conditions (high inlet geometric angles and low inlet Mach numbers), the bow shock waves are so wide that there is no intersection between them (Fig. 10). This observation suggests the existence of an upper limit for the generation of a collective shock; employing the assumption that detached waves are asymptotic to the free-stream Mach lines at large distances from the leading edge,[59] this upper limit can be estimated through Eq. (1). By re-arranging the system of equations in an alternative form [Eq. (2)], we can further deduce that the formation of a collective shock and the unique incidence problem are mutually exclusive since they, respectively, require supersonic and subsonic axial Mach numbers. This point also sheds light on why collective shocks have been overlooked in supersonic turbines: In mainstream applications, such as ORC systems and rocket engine turbopumps, the axial Mach numbers at the inlet of the supersonic blade rows are subsonic; on the contrary, recent developments in the field of rotating detonation engines foresee the possibility of a supersonic axial Mach number at the inlet of the first high-pressure stage,[19,60]

$$\begin{cases} \sin \mu = 1/M_{in} \\ \mu < \pi/2 - (\beta_g + i) = \pi/2 - \alpha_{in}, \end{cases} \tag{1}$$

$$M_{in} \cos(\alpha_{in}) = M_{in-axial} > 1. \tag{2}$$

2. Stability and hysteresis of a collective shock

Section III A 1 describes the process of the formation of a collective shock, but the unstarting of the supersonic channel is still not ensured, and it is determined by the stability of a collective shock outside the blade-to-blade channel. Downstream of the weak or strong collective shock, the axial Mach number becomes subsonic, enabling acoustic waves and pressure disturbances to travel upstream and impact the shock interface. These disturbances displace the shock wave, and its ability to return to its original position depends on its stability.

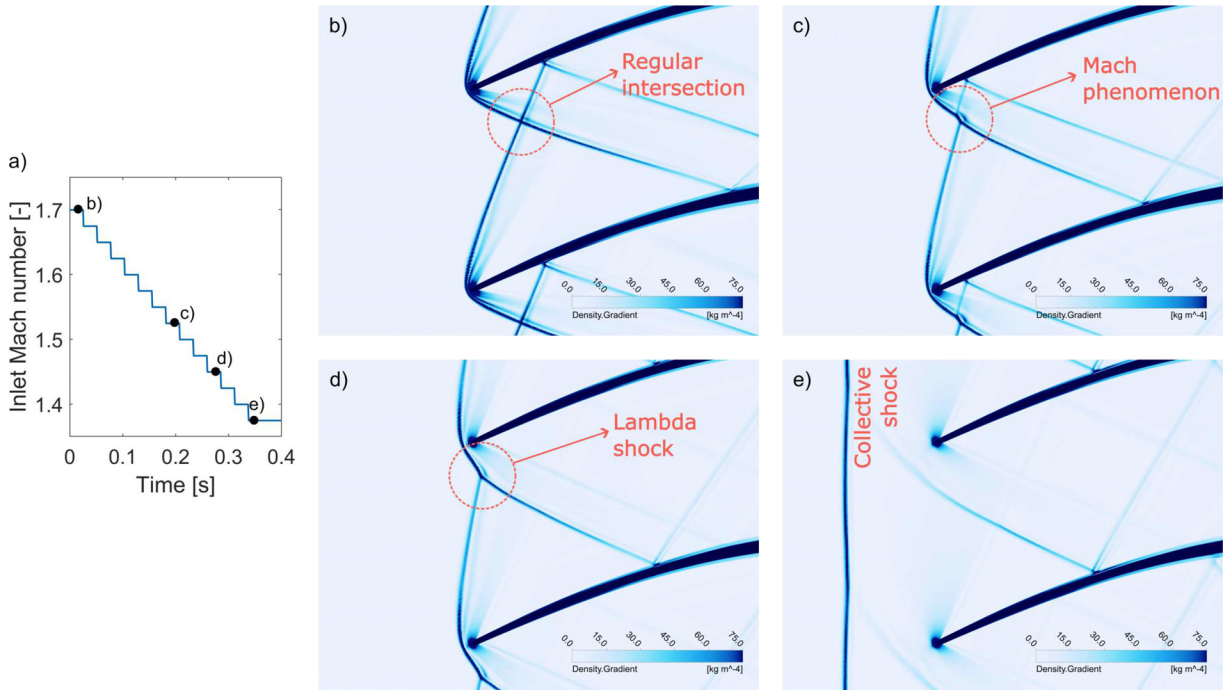

FIG. 9. Sequence of shock structures as the inlet Mach number is gradually reduced (a): there are a regular intersection (b), a Mach reflection (c), a lambda shock (d), and finally a collective shock (e). The inlet flow angle is always aligned to the profile inlet geometric angle.

The displacement z_s' of a plane shock wave inside a supersonic channel due to the pressure disturbance p' was determined by Culick and Rogers[61] assuming a quasi-steady behavior of the shock and isentropic flow conditions [Eq. (3)]. If the pressure disturbance is nonzero for a finite span of time, the displacement will decay to zero if τ is positive (stable shock) and will grow indefinitely if τ is negative (unstable shock),

$$\begin{cases} z_s' = \dfrac{D}{\tau} e^{-t/\tau} \displaystyle\int_0^t e^{t'/\tau} p'(t')\,dt' \\ \tau = \dfrac{1}{C_{in}} \left(\dfrac{1}{A} \dfrac{dA}{dz} \right)^{-1} \dfrac{2(\gamma+1)\bar{M}_{in}}{(\gamma-1)\left(1+\dfrac{\gamma^2+1}{\gamma-1}\right)\bar{M}_{in}^2}. \end{cases} \tag{3}$$

Since the sign of τ is determined by the cross-sectional area variation (dA/dz), the stability of the collective shock is influenced by the characteristics of the inlet channel, which spans from the inlet boundary to the leading edge of the blade. If the inlet channel is converging [Fig. 11(a)], the collective shock becomes unstable (negative τ) and it marches upstream: This behavior is ultimately responsible for the unstarting of the supersonic channel. The straight inlet channel [Fig. 11(b)] represents a limit case: The shock is neutrally stable and has no preferred position.[61] During the formation of a collective shock, the bow shock waves coalesce, and the merged shock is ejected from the blade-to-blade channel; this consideration implies that the collective shock is already moving: The neutrally stable behavior will not be able to stabilize it, and the shock will continue to march upstream. Finally, in the diverging channel [Fig. 11(c)], the collective shock stabilizes

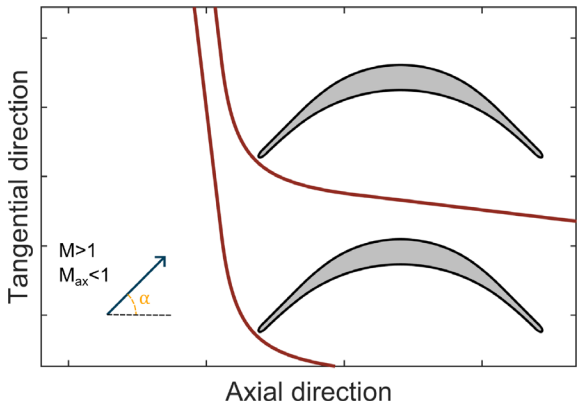

FIG. 10. High inlet geometric angles and low inlet Mach numbers prevent the formation of a collective shock, since there is no intersection between the bow shock waves.

(positive τ) in front of the supersonic blade row. While the formation of the collective shock can adversely affect the aerodynamic performance of the supersonic turbine, the unstarting of the supersonic channel with the unstarting shock marching upstream is deeply concerning since it can impact the overall gas turbine operation.

The analysis of shock stability is further complicated by the boundary layer on the hub and shroud walls. Although the effect of boundary layer growth can be accounted for [Fig. 11(d)], boundary layer separation induced by the collective shock may lead to instability

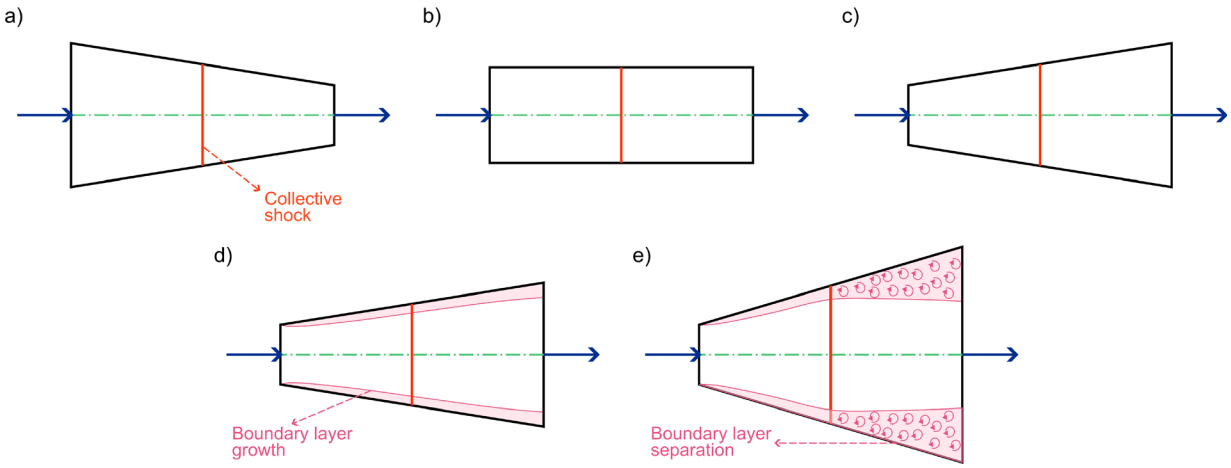

FIG. 11. Stability analysis of a collective shock inside a supersonic channel: (a) unstable shock in a converging duct, (b) neutrally stable shock in a straight channel, (c) stable shock in a diverging duct, (d) area contraction due to boundary layer growth, and (e) shock wave instability due to boundary layer separation caused by the collective shock.

[Fig. 11(e)]. In fact, a diverging channel is a necessary but not sufficient condition for a stable collective shock, and the isentropic assumption used in Eq. (3) is no longer valid. Given that a detailed study of the stability of plane shocks in supersonic channels is beyond the scope of this article, readers can refer to the works of Burgers,[62] Kantrowitz,[63] Hurrell,[64] and Culick[61] for more in-depth analysis.

Once again, the theoretical considerations presented above were confirmed by CFD simulations. Specifically, simulations were conducted on a straight and a diverging inlet channel, while the blade geometry is the same as Sec. III A 1.

In the straight channel simulation, the inlet Mach number was kept constant after the collective shock formation [Fig. 12(a)]. As predicted by the theory, the collective shock travels upstream and unstarts the supersonic channel [Figs. 12(b) and 12(c)]; the simulation is stopped when the shock reaches the inlet boundary.

The diverging case was chosen with a channel height ratio of 1.05 for two distinct reasons. First, since the simulations are quasi-3D with inviscid conditions on the hub and shroud walls, a positive τ is sufficient for the stability of the collective shock. Second, the formation of the collective shock for the considered geometry occurs at relatively low Mach numbers at the leading edge. Therefore, taking into account the flow acceleration in the diverging duct, even lower Mach numbers must be assigned at the inlet, and the minimum limit is set by the sonic condition.

The trend of the inlet Mach number was specifically conceived to assess if the collective shock is stable in a diverging channel and whether its formation exhibits a hysteretic behavior. To accomplish this, the inlet Mach number was systematically varied in three stages: gradual decrease, stability analysis with a constant value, and gradual increase in the inlet Mach number to investigate a potential hysteresis [Fig. 13(a)]. Additionally, shock motion was tracked by placing monitor points at intervals of 1 mm in the axial direction along the mid-pitch line; at each instant, the position of the shock corresponds to the coordinate with the maximum density gradient.[65]

The initial part of the simulation (not shown in Fig. 13) produces the same shock structures described in detail in Sec. III A 1 and displayed in Fig. 9. At point c, a reduction in the inlet Mach number results in the formation of the collective shock. In the next steps, further reductions or increments of the Mach number shift the shock further or closer to the leading edge. The stability of the collective shock in a diverging channel is demonstrated by these variations because after each step the collective shock moves and finds a new equilibrium position; this point is extremely evident, especially in the prolonged step at the lowest inlet Mach number [Fig. 13(d)], where the collective

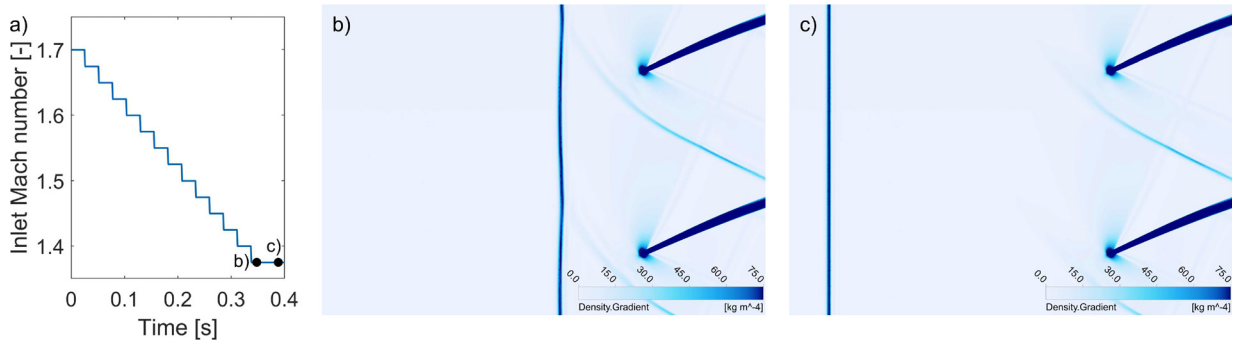

FIG. 12. Collective shock unstarting in a straight inlet channel. (a) the prescribed inlet Mach number trend and (b) and (c) the corresponding shock wave position.

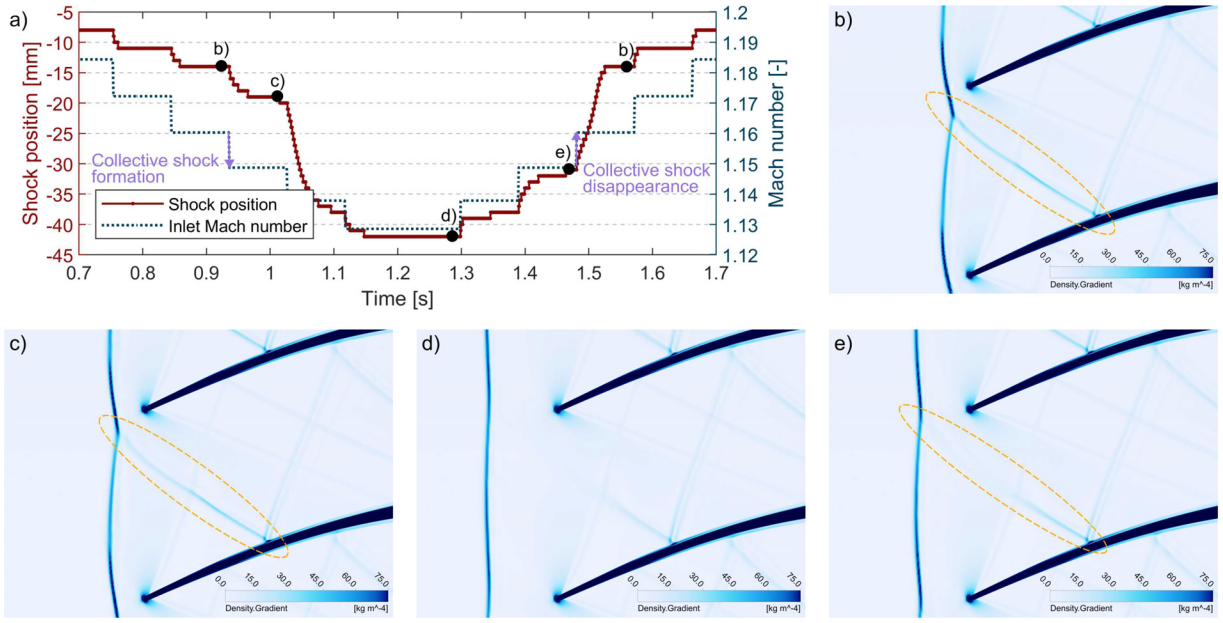

FIG. 13. Stability and hysteresis of a collective shock in a diverging channel. (a) The prescribed inlet Mach number trend and the associated shock wave position. (Negative values on the y axis correspond to a position upstream of the leading edge.) The asymmetry in shock motion is examined through the shock structures shown in (b), (c), (d), and (e).

shock is stationary for a relatively large amount of time. Furthermore, it is noteworthy that the response time of the collective shock to inlet condition variation is longer compared to the time required for the bow-shock waves to reach the new equilibrium position. This observation led to the adoption of a longer step in this simulation ($\Delta t = 0.09$ s) compared to the previous one [Figs. 9(a) and 13(a)].

The formation and disappearance of a collective shock occur at the same inlet Mach number; this characteristic is highlighted by Fig. 13(b), which is identical along the decreasing and the increasing ramp. Therefore, the starting and unstarting of a supersonic inlet turbine due to collective shocks can be characterized by a single curve. However, there is an asymmetry in the motion of the collective shock during the reduction and the following increase in the inlet Mach number. This behavior can be attributed to the residual effect of the right branch of the bow shock wave, which is detached during the formation of the collective shock [Fig. 13(b)]. This branch does not immediately vanish and affects the motion of the shock waves [Fig. 13(c)]. When the inlet Mach number is increased again, the right branch gradually re-gains strength, but the intensity and the position of the residual shock are different for the same inlet Mach number [Figs. 13(c) and 13(e)]. Nonetheless, this feature is temporary and of limited practical interest, while the most relevant outcome of this analysis is that the detachment of the right branch of the bow shock wave with collective shock formation and its reattachment with collective shock disappearance coincide.

B. A reduced order model to predict the formation of a collective shock

The formation of a collective shock can result in the unstarting of a supersonic turbine, which can have severe consequences (Sec. III A). Avoiding this additional unstarting mechanism represents a prerequisite for the correct operation of these machines, and it should be accounted for already in the preliminary design stages. However, during this early stage, the amount of data available is limited, and a CFD-based approach would be computationally impractical to investigate a large design space in search of optimal operating conditions and turbine geometry.

To predict the formation of a collective shock with limited data, a model based on a simple criterion is necessary. The selected criterion is as follows: The formation of a collective shock will occur when the axial coordinate of the intersection point between the bow shock waves is located on the line that connects the leading edges of the blade row. This straightforward criterion will prove to be quite effective (Sec. III B 3), but it requires an accurate prediction of the bow shock wave generated by the leading edge.

Moeckel developed an approximate method to predict the location of detached shock waves ahead of two-dimensional and axially symmetric bodies by applying the continuity relation on the sonic line.[59] To approximate the problem to an equivalent one-dimensional form, the following assumptions are made: (I) The form of the detached wave from the axis to its sonic point S is represented by a hyperbola asymptotic to the free stream Mach lines (Fig. 14); (II) the line tangent to the body in the sonic point SB has an inclination equal to the detachment angle; and (III) the sonic line (S-SB) is straight and inclined at an angle that depends only on the free stream Mach number. Considering these hypotheses, this methodology struggles with extremely blunt bodies and fails in the vicinity of sonic conditions.

Although Moeckel originally intended his methodology to be applied only to the portion of the shock between the foremost point and the sonic one, Love[66] later suggested that it could provide

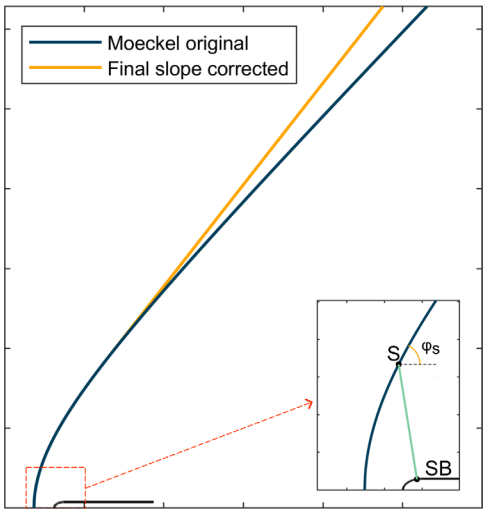

FIG. 14. Comparison between the bow shock shape predicted by Moeckel's original model and its improved version for the final slope. The bottom right corner features a zoomed-in view of the leading-edge area, displaying the sonic point on the body (SB), the sonic point on the shock (S), and the straight sonic line, as assumed by Moeckel's model.[59]

satisfactory results for certain nose shapes even at distances well beyond the sonic point. However, as shown in Fig. 15(a), a miscalculation on the slope of the bow shock wave can significantly impact the determination of the intersection point between the bow shock waves, especially in cases where large pitch to leading edge thickness ratios are needed to minimize shock losses. Furthermore, Moeckel's model accounts for asymmetrical bow shocks resulting from incidence angles at the leading edge, but as depicted in Fig. 15(b), its prediction for large incidence angles deviates significantly from the actual shock structure.

1. Asymptotic slope of a bow shock wave

The bow shock wave predicted by Moeckel's model is asymptotic to the free stream Mach line at large distances from the leading edge. This description is valid only for extremely weak shock waves with infinitesimal flow deflection, i.e., for a bow shock wave that behaves as a Mach wave. However, a bow shock, in the general case, has a finite strength and induces flow deflection. To address this inconsistency and to determine the asymptotic slope of the hyperbolic curve, it is proposed an analogy between a bow shock and an oblique shock generated by a sharp corner (Fig. 16).

To solve the analogy, it is crucial to establish a relationship between the corner angle θ and the bow shock wave. Once this connection is determined, the closed analytical solution of the inviscid corner problem can be used to calculate the asymptotic slope of the bow shock. In a corner problem, when we increase the inlet Mach number while keeping the corner angle θ fixed, the slope of the oblique shock progressively decreases. This same behavior is observed in bow shock waves, although the decrease in slope is slower compared to the corner problem. To understand this characteristic, it is important to consider that, as the inlet Mach number increases, the distance between the leading edge and the foremost point of the shock, denoted as X_0 in Fig. 16, decreases; as a result, from the perspective of an

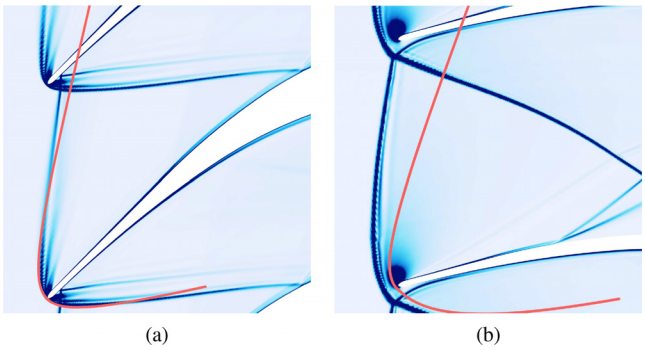

FIG. 15. Comparison between the bow shock shape extracted from CFD simulations (density gradient in background) and the shape predicted by Moeckel's model (solid line in foreground): (a) M = 1.92, β_{g-in}=45°, i = 0° and (b) M = 2.2, β_{g-in}=15°, i = 25°.

observer situated at X_0, the angles described by the lines connecting X_0 to each point of the leading edge become larger. To incorporate this property of bow shock waves into the analogy, when the inlet Mach number is increased, the corresponding corner angle θ will not remain constant even if the leading-edge geometry remains fixed. Equation (4) proposes a correlation to close the analogy, where ϕ_s is the local inclination of the bow shock in the sonic point relative to an axis aligned to the leading edge, and k is an empirical parameter that depends on the specific heat ratio (with the hypothesis of perfect gas behavior) and the leading-edge shape,

$$\theta = \frac{\frac{\pi}{2} - \phi_s(M,\gamma)}{k(\gamma, shape)}. \tag{4}$$

The calibration of the constant k [Eq. (4)] necessitates a CFD simulation that considers the specific heat ratio and leading-edge shape relevant to each application. However, the computational cost of conducting a single simulation with a simple geometry is quite limited, enabling the practical application of the proposed correlation.

To validate the model, a series of CFD simulations were performed on an isolated profile consisting of two straight lines separated by the thickness value and closed by various leading-edge shapes. In Fig. 17, the results for an elliptic leading edge with a semiaxis ratio of 3.2 (a typical value for supersonic profiles[23]) and a specific heat ratio

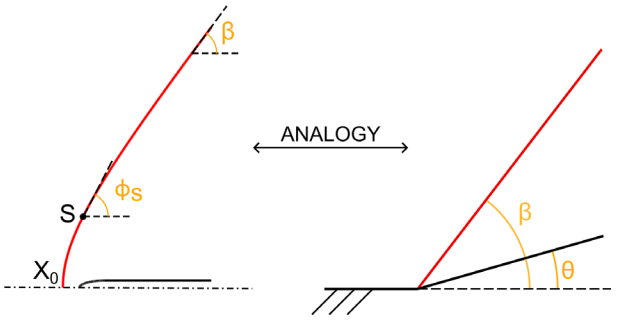

FIG. 16. Analogy between the bow shock generated by the leading-edge and the oblique shock generated by a sharp corner.

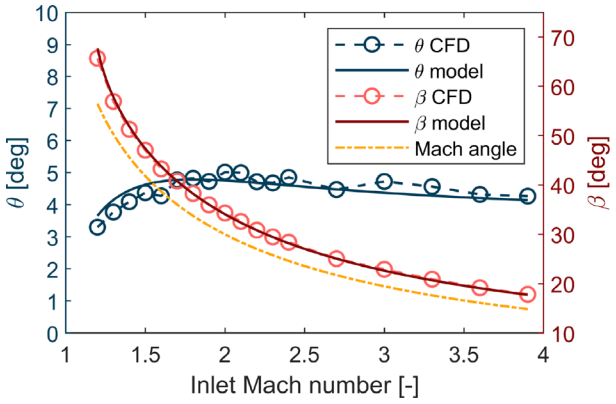

FIG. 17. Comparison between the corner angle θ and the asymptotic shock slope β predicted by the model (solid lines) and the numerical values extracted from CFD simulations (dotted lines), where each circle corresponds to a CFD simulation. The leading-edge shape is an ellipse with a semiaxis ratio of 3.2, and the specific heat ratio is 1.4.

of 1.4 are depicted. The asymptotic slope of the bow shock (β CFD) is extracted through image postprocessing techniques, and then, oblique shock relations[57] are applied to calculate the corresponding θ (θ CFD). The discrepancy between θ predicted by the model and the one derived from CFD simulations is below 0.5° across the entire Mach range; in addition, the proposed correlation accurately reproduces the trend observed in the CFD simulations, demonstrating its effectiveness. The asymptotic slope angle β predicted by the model closely aligns with the numerical results, representing a considerable improvement over the Mach angle employed in Moeckel's original methodology.

Additional simulations were conducted to examine the performance of the correlation on three different leading-edge shapes: a highly eccentric ellipse with a semiaxis ratio of 7, a circle (a/b = 1), and a square shape (Fig. 18). The correlation demonstrates excellent performance for highly eccentric geometries [Fig. 18(a)], with minimal differences and accurate prediction of trends. In the case of a circular leading edge [Fig. 18(b)], the results are still satisfactory in terms of shock angle β, although the correlation is less accurate for Mach numbers below 2. However, for the square shape [Fig. 18(c)], the trend predicted by the correlation does not align with the numerical results. This discrepancy arises due to the inherent limitation of the correlation, which becomes less accurate as the leading-edge bluntness increases. This limitation is inherited through the sonic angle ϕ_s from Moeckel's model itself, which, as stated by the author himself, exhibits the highest accuracy for "bodies only slightly blunter than the wedge or cone." Despite this limitation, the shock angle β predicted by the model consistently represents a substantial improvement over the Mach angle, even in the case of a square leading edge.

The impact of the specific heat ratio was also investigated [Figs. 17 and 18(d)], revealing that lower specific heat ratios correspond to smaller θ angles; nonetheless, the correlation accurately captures these variations.

Furthermore, it is relevant to notice that the leading-edge shape significantly affects the constant k; for instance, the value of k varies from 7.2 for the highly eccentric ellipse to 3.4 for the square shape.

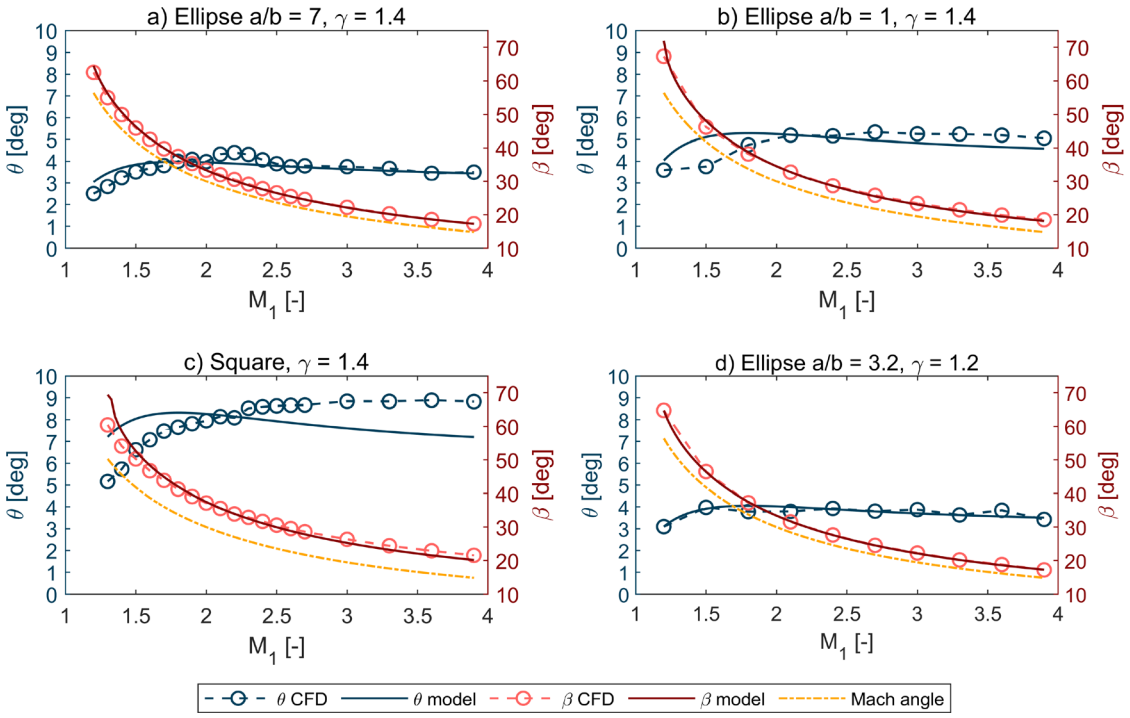

FIG. 18. Comparison for various leading-edge shapes (a)–(c) and specific heat-ratios (d) between the corner angle θ and the asymptotic shock slope β predicted by the model (solid lines) and the numerical values extracted from CFD simulations (dotted lines), where each circle corresponds to a CFD simulation.

Conversely, the influence of the specific heat ratio is relatively modest, ranging from 5.98 to 5.91 for a variation of γ from 1.4 to 1.2. The limited impact of the specific heat ratio can be explained by examining Eq. (4): While the leading-edge shape is solely represented by the constant k, a variation in the specific heat ratio also alters the angle ϕ_s at the sonic point, thereby mitigating its effect on k. In conclusion, Fig. 19 illustrates a comparison between the original methodology of Moeckel and the improved version for the asymptotic slope of the bow shock wave. The improved version demonstrates a clear enhancement in accuracy, which will be beneficial for the calculation of the unstarting limit curves caused by the formation of a collective shock.

2. Model correction for large incidence angles

The incidence angle at the leading edge produces an asymmetrical bow shock wave, and Moeckel's model accounts for this effect by shifting the position of the sonic point on the body; this technique provides acceptable results for limited incidence angles, but, as displayed in Fig. 15, the predicted shapes are unsatisfactory for large incidence angles (above 10°).

From a physical perspective, the flow observes an increased leading-edge thickness at large incidence angles. This is because the flow encounters obstruction not only from the conventional leading-edge thickness (segment AG in Fig. 20) but also from a portion of the pressure side (or suction side) for positive (negative) incidence; this additional contribution increases the overall thickness (segment GF).

Equation (5) presents a correlation that provides an estimation of the effective leading-edge thickness observed by the flow. The development of this correlation involved two steps: First, it was calculated the segment GF responsible for the increase in thickness, and then, the two contributions (AG and GF) were projected toward the normal direction of the flow. It is relevant to notice that in the calculation of GF, only the top half pitch was considered because the influence of the lower half is limited since most of the flow is likely to turn before reaching the upper blade. The specific choice of considering half pitch, instead of smaller or larger values, was primarily motivated by the good agreement observed with the results,

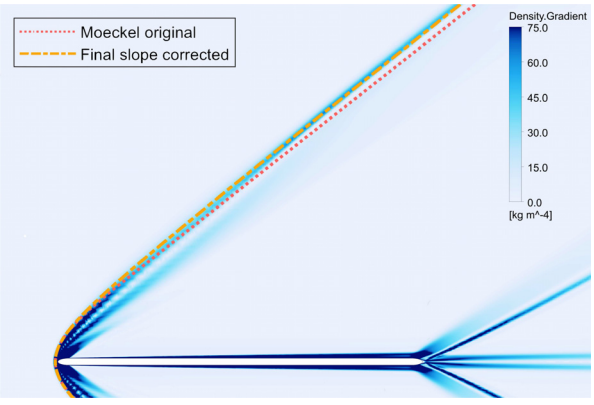

FIG. 19. Comparison between the original methodology of Moeckel and the improved version for the asymptotic slope of the bow shock wave. The leading-edge shape is an ellipse with a semiaxis ratio of 3.2, the specific heat ratio is 1.4, and the inlet Mach number is 1.8.

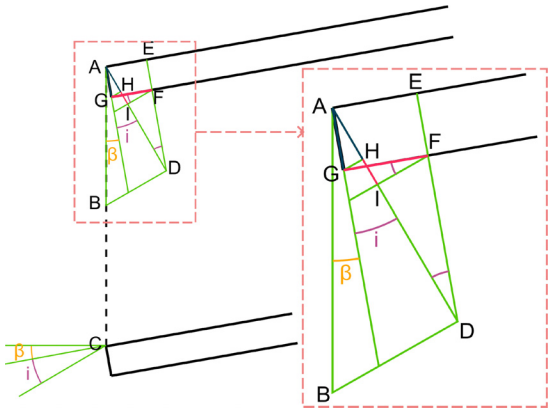

FIG. 20. The sketch displays the projections that are behind the development of the leading-edge thickness correction [Eq. (5)].

$$\begin{aligned} th_{corr} &= \overline{AH} + \overline{HI} = \overline{AG}\,\cos(i) + \overline{GF}\,\sin(i) \\ &= \overline{AG}\,\cos(i) + \overline{AD}\,\sin^2(i) \\ &= \overline{AG}\,\cos(i) + \overline{AB}\,\cos(\beta_g + i)\,\sin^2(i) \\ &= th\,\cos(i) + \frac{g}{2}\cos(\beta_g + i)\,\sin^2(i). \end{aligned} \tag{5}$$

Figure 21 illustrates the trend of the corrected thickness for three different inlet geometric angles. When the incidence angle is zero, the corrected thickness is naturally equal to the leading-edge thickness. At small incidence angles, the effect of incidence is limited, which explains why Moeckel's model continues to perform well within this range. However, for large incidence angles, the "observed" thickness experiences significant growth, with the corrected thickness reaching values nearly three times larger than the leading-edge metallic thickness. Moreover, an increase in the inlet geometric angle diminishes the impact of the incidence angle. This observation aligns with the physical understanding of the problem: As the inlet geometric angle increases, the portion of the profile observed by the flow (segment GF) becomes smaller. This observation will be further supported by the results presented in Sec. III B 3.

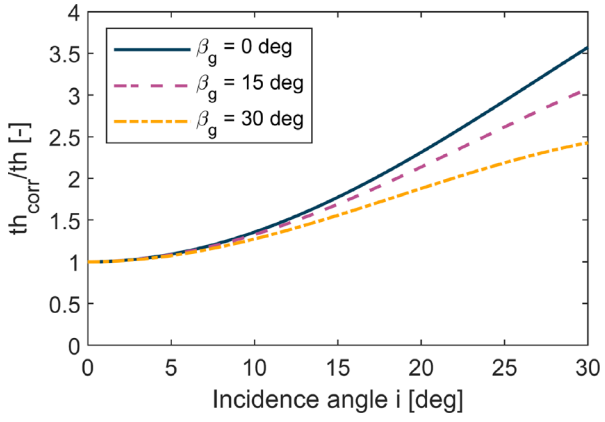

FIG. 21. Trend of the corrected thickness with incidence angle for three different inlet geometric angles.

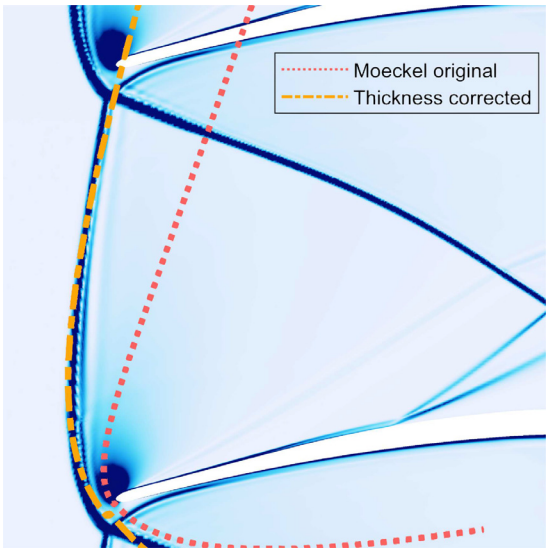

FIG. 22. Comparison between the original methodology of Moeckel and the improved version incorporating the thickness observed by the flow. The inlet Mach number is 2.2, the inlet geometric angle is 15°, and the incidence angle is 25°.

Finally, Fig. 22 showcases the bow shock wave generated using the updated model incorporating both the leading-edge thickness and final slope corrections. The enhancement over the baseline is remarkable, particularly for large incidence angles. Additionally, it is noteworthy the increased distance between the leading edge and the bow shock wave at large incidence angles, providing further confirmation that the thickness observed by the flow is indeed greater.

3. Collective shock unstarting curves and model verification

The unstarting limit of the collective shock is influenced by several factors [Eq. (2)],

$$unstart = unstart(M_{in},\ \beta_{g-in},\ i,\ g/th,\ shape,\ \gamma). \tag{6}$$

Among these variables, the first four exert a dominant influence on the unstarting value, while the impact of the latter two is of secondary importance (Fig. 23 and Sec. III B 1). Hence, the leading-edge shape and the specific heat ratio were kept constant throughout the verification process; specifically, an elliptic leading edge with a semi-axis ratio of 3.2 and a specific heat ratio of 1.4 were selected.

CFD simulations are necessary to verify the unstarting curves predicted by the model. However, considering the number of parameters and the large number of evaluations required, performing time-accurate CFD simulations would be prohibitively expensive and unnecessary. As emphasized in the preceding section, this study focuses on collective shock unstarting from a quasi-steady standpoint, rendering time accuracy superfluous. Therefore, a procedure based on consecutive steady-state simulations was devised, whereby only one parameter is altered while keeping all others constant.

To illustrate the process, let us consider calculating the unstarting Mach number for a specific geometry and flow angle. The initial Mach number is sufficiently high to ensure that the supersonic profile is in a started operating mode; as demonstrated in Sec. III A 2, beginning

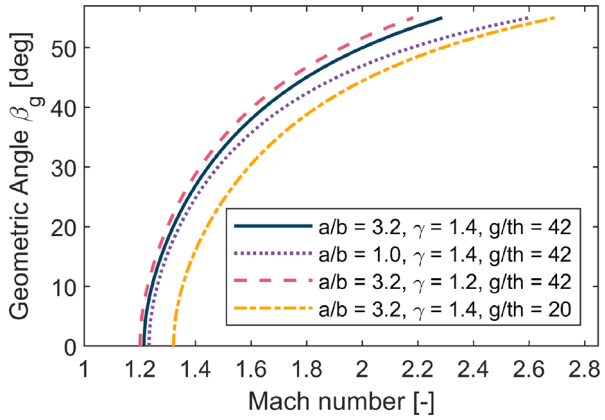

FIG. 23. Sensitivity of the unstarting limit induced by collective shock formation to variations of the ellipse semi-axis ratio, specific heat ratio, and pitch to leading-edge thickness ratio.

from a started or an unstarted condition does not affect the results since the phenomenon is not hysteretic with respect to the inlet conditions. Since the choice of the inlet channel is arbitrary, it was selected a straight duct, because for this geometry, the formation of the collective shock can be clearly identified by the shock moving upstream. After each steady-state simulation, the inlet Mach number is reduced by ΔM, while employing the solution of the previous simulation to initialize the subsequent one. The iterative procedure continues until a collective shock is generated ahead of the blade row and begins propagating upstream in the time-marching steady-state solver. The ΔM for the inlet Mach number is 0.025, and the Δi for the incidence angle is 2°; in the authors' opinion, these values represented an acceptable compromise between accuracy and simulation time.

The results of the procedure based on steady-state simulation were preliminarily compared to time-accurate unsteady simulations with a stepwise trend for the inlet conditions. The cascade geometry employed for the verification of the procedure is the same as Sec. III A 1. As demonstrated by the results reported in Table I, the difference in the unstarting values between the two approaches falls within ΔM (or Δi), confirming that the approach can be reliably employed for the determination of the unstarting limits while optimizing computational resources.

Figure 24 provides a comparison of the unstarting limit curves, illustrating the relationship between the inlet Mach number and the inlet geometric angle for two different leading-edge thickness to pitch ratios. The trends observed indicate that higher inlet Mach numbers allow for larger inlet geometric angles, while an increase in the leading-edge thickness reduces the available design space.

To understand these trends, it is important to remember that a collective shock is generated from the coalescence of the bow-shock waves, which for our simple criterion happens when their intersection is placed at the leading-edge axial coordinate. Higher inlet Mach numbers reduce the asymptotic slope of the bow shock, pushing the intersection point further downstream and minimizing the risk of unstarting. Conversely, an increase in the inlet geometric angle is detrimental: It does not affect the shape of the bow-shock waves, but it shifts the position of the intersection point closer to one of the leading edges and consequently closer to the leading-edge line [Figs. 24(a) and

TABLE I. Comparison between the unstarting limits found, respectively, by the procedure based on consecutive steady-state simulations and the unsteady simulation with a stepwise trend of the inlet conditions.

	Steady-state simulations	Unsteady simulation
$M_{unstart}$ (-) ($\Delta M = 0.025$)	1.37	1.36
$i_{unstart}$ (°) ($\Delta i = 2°$)	16.0	16.0

24(b)]. Furthermore, a higher leading-edge thickness to pitch ratio amplifies the influence of the subsonic region of the bow shock. This feature affects the space required to reach the asymptotic slope (hyperbolic shape), brings forward the intersection between bow shock waves, and ultimately facilitates collective shock unstarting.

The unstarting curves generated by the model exhibit excellent agreement with the CFD results. This can be attributed to the model's ability to accurately identify the condition for bow shock merger and the improved prediction of bow shock wave shape through the correction of the asymptotic slope. However, it should be noted that the model slightly overestimates the unstarting condition at large inlet geometric angles. This discrepancy arises because small inaccuracies in the bow shock wave at high inlet geometric angles have a more pronounced impact on the precise location of the intersection point [Fig. 24(b)].

Figure 25 displays the effect of the incidence angle on the unstarting limit for three values of the inlet geometric angle (0°, 15°, and 30°). When the flow encounters a profile at a non-zero incidence angle, it generates an asymmetrical bow shock wave at the leading edge of the blade. As the incidence angle increases, one branch of the shock wave moves upstream more rapidly, promoting the formation of a collective shock [Figs. 25(a) and 25(b)]. However, this phenomenon can be alleviated by having less inclined bow shock waves, which require higher inlet Mach numbers.

The influence of the incidence angle becomes less pronounced at higher inlet geometric angles, which aligns with the trend observed in Eq. (5) (Fig. 21). It is noteworthy that the difference between the unstarting curves with and without incidence angle is significant at a 0° inlet geometric angle, but considerably smaller at a 30° inlet geometric angle.

The unstarting curves generated by the model closely match the results obtained from CFD simulations. The agreement is excellent for the 0° inlet geometric angle, but the model underestimates the unstarting values for non-zero inlet geometric angles. This discrepancy can be attributed to the thickness correction, particularly in relation to the length of pitch considered in the calculation of segment GF (Fig. 20). Introducing an additional variable to account for the variation of pitch based on the inlet geometric angle could improve the accuracy, but it would also complicate the model and make its practical application more challenging. Moreover, it is important to note that the model's underestimation falls on the conservative side in terms of unstarting, reducing the criticality of this issue.

In conclusion, the reduced order model captures accurately the variations of the primary four variables and the agreement with the CFD results is within 0.05 for the Mach number and 3° for the incidence angle. Moreover, the model's simplicity enhances its practical value as it can be readily incorporated into a mean-line code for the preliminary design of supersonic blade rows.

IV. KANTROWITZ UNSTARTING

A. Description of the unstarting mechanism and extension of the classical theory

A supersonic diffuser is typically characterized by a converging–-diverging shape. The starting of this geometry leads to the formation of a normal shock in the converging section, which is expelled from the diffuser for stability reasons[61] (see Sec. III A 2). To establish a supersonic flow and swallow the normal shock, a significant increase in the inlet Mach number becomes necessary. Kantrowitz and Donaldson[41] discovered an analytical relationship [Eq. (7)] that determines the minimum inlet Mach number required to self-start a diffuser with a contraction ratio of A/A^*,

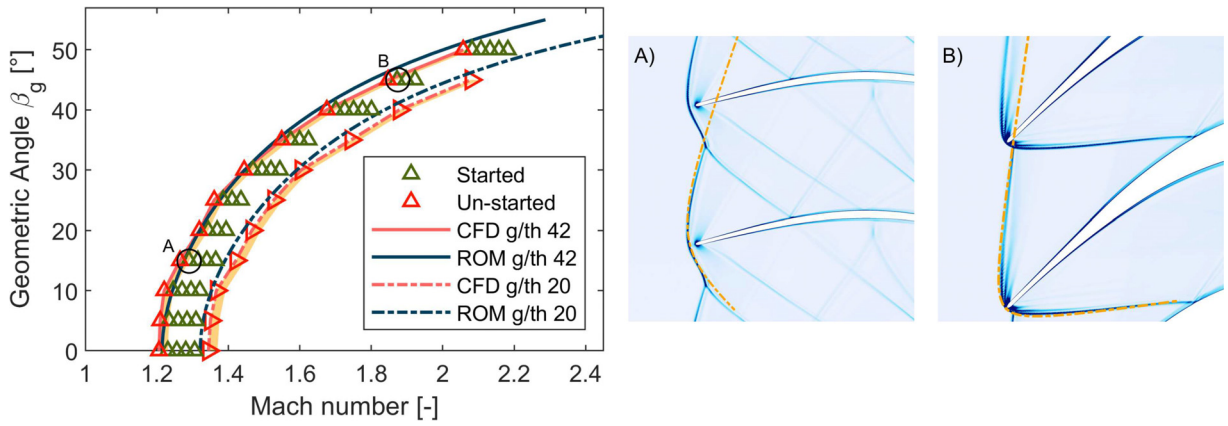

FIG. 24. Unstarting limits induced by collective shock formation as a function of the inlet Mach number, inlet geometric angle, and leading-edge thickness to pitch ratio. The red brighter lines represent CFD results, while the blue darker lines indicate the predictions of the reduced order model. The green and red triangles correspond, respectively, to started and unstarted turbine operation. (The green triangles are displayed only for the highest leading-edge thickness to pitch ratio case.) The yellow-filled area represents the range between the last started condition and the unstarted condition for the CFD simulations. Frames (a) and (b) illustrate the shock structures for a low and high inlet geometric angle, accompanied by the model-predicted bow shock shape displayed as a dashed line.

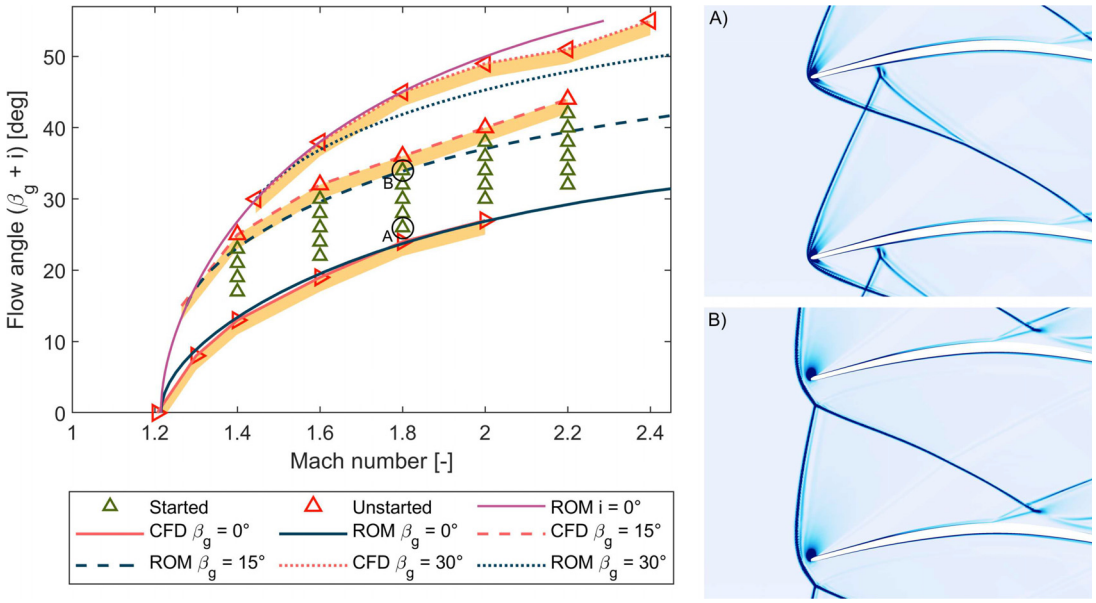

FIG. 25. Unstarting limits induced by collective shock formation as a function of the inlet Mach number, inlet geometric angle, and the incidence angle. The red brighter lines represent CFD results, while the blue darker lines indicate the predictions of the reduced order model. The green and red triangles correspond, respectively, to started and unstarted turbine operation. (The green triangles are displayed only for the case with an inlet geometric angle of 15°.) The yellow-filled area represents the range between the last started condition and the unstarted condition for the CFD simulations. Frames (a) and (b) illustrate the shock structures for a low and high incidence angle.

$$\begin{cases} \left.\dfrac{A^*}{A_{in}}\right|_{self-started} > \left(\dfrac{\dfrac{\gamma+1}{2}}{1+\dfrac{\gamma-1}{2}M_n^2}\right)^{\frac{\gamma+1}{2(\gamma-1)}} \\ M_n^2 = \dfrac{(\gamma-1)M_{in}^2+2}{2\gamma M_{in}^2-(\gamma-1)}. \end{cases} \tag{7}$$

Equation (7) was derived under the assumption of quasi-one-dimensional flow, and it considers that the normal shock is swallowed when the post-shock flow reaches sonic conditions in the throat. Once the diffuser is started, the inlet Mach number can be reduced, and unstarting will occur only if sonic conditions are reached in the throat by the free stream flow. This hysteretic behavior of the Kantrowitz limit defines three regions (Fig. 26): the self-started region, the unstarted region, and a region exhibiting dual behavior where the diffuser can either start or unstart depending on the initial conditions.

The starting of a supersonic intake is of extreme importance for a successful operation of a supersonic aircraft. To enhance our comprehension of this process, significant research efforts have been dedicated to verify experimentally the Kantrowitz criterion. Moreover, additional theories proposed by Veillard *et al.*[67] and Flock and Gülhan[68] have expanded upon the original methodology. However, when it comes to applying these findings to supersonic blade rows, the research efforts have been relatively limited and, since the time of Kantrowitz himself,[43] the original limit has persisted in the design of supersonic blade rows.

The original theory, while valuable, relies on assumptions that may not be as applicable in turbomachinery applications. First, the theory assumes that the shock in the unstarted configuration is always a normal shock. However, as explained in Sec. III A 1 concerning the collective shock, this holds only when the flow is completely axial. In all other cases, despite appearing normal to the channel axis due to the periodicity of a blade row, the unstarting shock takes the form of an oblique shock wave (Fig. 8). The unstarting shocks generated by the two unstarting mechanisms are different: The collective shock results from the merger of the bow shock waves, whereas Kantrowitz's unstarting shock appears when sonic conditions are reached in the converging section of a duct (before the throat). Additionally, it is also important to note that this discussion does not include the effect of the incidence angle (the inlet geometric angle and the inlet flow angle coincide).

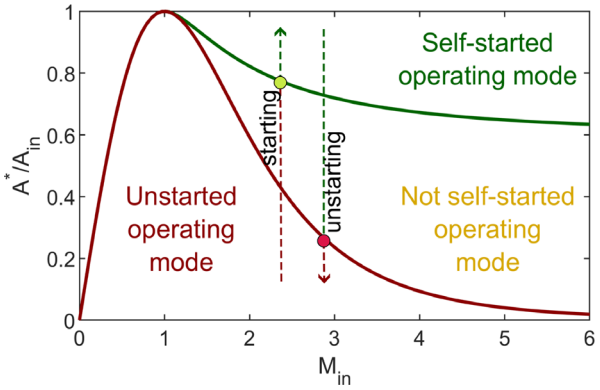

FIG. 26. Contraction ratio A/A^* allowed by the Kantrowitz limit at varying inlet Mach number. The hysteresis between the starting and unstarting condition is highlighted by upward and downward arrows, respectively.

The behavior of the unstarting shock is influenced by the inlet Mach number and the inlet flow angle. Depending on these factors, the unstarting shock can manifest as a weak or strong oblique shock wave. In the case of a strong oblique shock wave, the Mach number downstream of the shock becomes subsonic. As the flow progresses through the converging blade-to-blade channel, it undergoes acceleration. If sonic conditions are achieved in the throat, the strong oblique shock is effectively swallowed by the turbine, resulting in a supersonic flow from the inlet to the outlet.

On the contrary, the case of a weak oblique shock presents a more distinct behavior. Downstream of a weak oblique shock, the Mach number remains supersonic (except for a small region near θ_{max}). If the inlet Mach number is not sufficiently high to start the blade row, leading to the formation of a weak oblique shock, the lower but still supersonic Mach number downstream of the weak oblique shock is certainly insufficient for the starting. Hence, the weak oblique shock alone fails to provide a consistent representation of the flow; to fully describe this scenario, it becomes necessary to introduce a second set of shock waves. From the authors' perspective, these additional shock waves manifest as normal shock waves positioned at the entrance of the blade-to-blade channel. This explanation finds support in the shock structures observed during the quasi-steady initiation of a supersonic blade row under weak oblique shock conditions (Fig. 27).

Figure 28 displays the procedure implemented for the calculation of the maximum contraction ratio A/A^*, which is defined as the ratio between the inlet area and the throat area. The logic behind the three cases is the following: A supersonic flow with an inlet Mach number M_{in} and an inlet flow angle α_{in} are assigned at the inlet; then, the flow undergoes a transition from supersonic to subsonic due to the presence of shock waves produced during the starting process; finally, the subsonic flow is isentropically accelerated within the converging blade-to-blade channel until sonic conditions are attained in the throat. In essence, the underlying principle is very similar to the original Kantrowitz theory, with the distinction that normal shock waves were substituted by a more consistent shock selection.

These procedures were utilized to conduct a comprehensive parametric analysis, and the results are illustrated in Fig. 29. The figure demonstrates that the proposed methodology expands upon the original Kantrowitz theory, with the Kantrowitz theory exclusively corresponding to the axis representing a zero-inlet flow angle. For each inlet flow angle, the minimum inlet Mach number corresponds to the weakest oblique shock wave, namely, the Mach wave. If smaller inlet Mach numbers are assigned in comparison with this condition, only a left-running oblique shock wave (increasing the relative Mach number) would yield a physically consistent solution. However, a detailed investigation of these cases falls beyond the scope of this study.

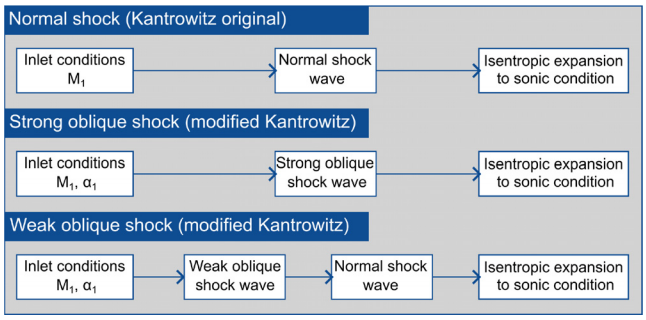

FIG. 28. Procedures implemented for the calculation of the maximum contraction ratio A/A^* given the inlet Mach number and the inlet flow angle. The original Kantrowitz methodology is extended to account weak and strong oblique shock waves positioned at the inlet of the supersonic blade row.

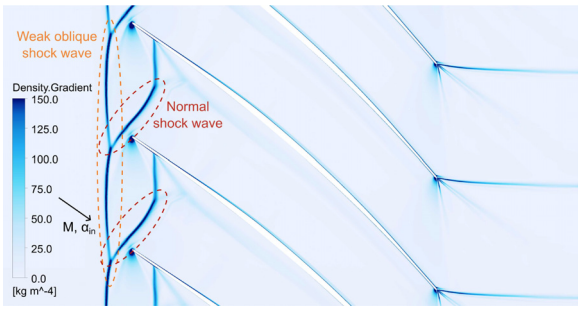

FIG. 27. Complex shock structure system ahead of the supersonic blade row for the weak oblique shock starting. From the flow perspective, the first set of shocks are weak oblique shock waves, while the second ones are normal shocks. It is noteworthy that the normal shocks induce boundary layer separation on the pressure side.

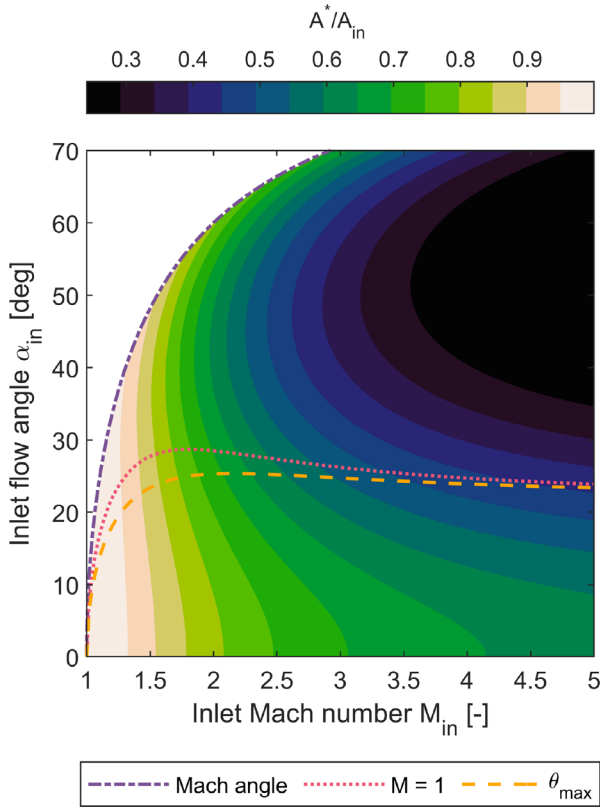

FIG. 29. Maximum contraction ratio A/A^* as a function of the inlet Mach number and the inlet flow angle calculated with the modified Kantrowitz methodology. The dash dotted line represents the Mach wave, the dotted line distinguishes supersonic flow from subsonic flow downstream the oblique shock, and the dashed line corresponds to the maximum flow turning induced by the shock.

It is noteworthy that there is a continuum of results between the weak and strong oblique shock cases, with the interface between the two represented by a dotted line denoting the sonic condition (M = 1) downstream of the shock. In both the strong and weak oblique shock cases, a higher inlet Mach number corresponds to a greater maximum contraction ratio that satisfies the self-starting condition of a supersonic blade row.

In the weak oblique shock case, the contraction ratios at increasing inlet flow angles do not exhibit a monotonic behavior. In fact, a region characterized by the highest maximum contraction ratios emerges. (Notice that Fig. 29 plots the reciprocal of the maximum contraction ratio; hence, the highest contraction ratios correspond to the darkest colors.) To explain this behavior, it is essential to consider that the total contraction ratio is a combination of two factors for an oblique shock: the turning induced by the oblique shock and the area contraction required to achieve sonic conditions in the throat.[68] As the inlet flow angle increases, the oblique shock turning diminishes due to the smaller shock angle (Fig. 29); simultaneously, the contraction ratio to reach sonic conditions enlarges because the Mach number behind the normal shock decreases. (The normal shock is stronger due to the higher Mach number behind the oblique shock.) Consequently, in this region, a favorable compromise is reached between the two factors, leading to the maximization of the contraction ratio.

B. The effect of boundary-layer separation on the self-starting Mach number

The contraction ratios calculated above provide a necessary condition for the self-starting of a supersonic turbine, but they do not guarantee it. These ratios determine whether the shock structures preceding the blade row will start advancing in the blade-to-blade channel. However, the aerodynamics of a supersonic cascade is considerably more complex than that of a conventional supersonic intake. In particular, the process of shock swallowing is highly critical for a supersonic blade due to the adverse pressure gradient created on the suction side as the shock begins to progress through the blade-to-blade channel. If the boundary layer separates because of this adverse pressure gradient, the effective area decreases, and the flow experiences deceleration. In cases where the separation is significant, the flow becomes choked, causing the shock wave to be expelled back to the inlet of the blade row instead of advancing downstream.

Two unsteady simulations were carried out to highlight the influence of shock-induced boundary layer separation during the starting process. In each simulation, the initial condition was subsonic with an inlet Mach number of 0.1. Subsequently, the Mach number was increased with a single step to 2.5 and 3.4, respectively (impulsive starting). The geometry selected for the analysis has an inlet geometric angle of -35° and an outlet geometric angle of -56.4°; the starting condition for this geometry (corresponding to the weak oblique shock case) demands a minimum inlet Mach number of 2 for the shock swallowing. As the simulations were time accurate, residual convergence was ensured at each time step (see Sec. II for more details).

Figure 30 displays five instants of the successful starting of a supersonic blade row when the inlet Mach number was raised to Mach 3.4. When the inlet conditions are changed with a step, three phenomena are produced, which are explained as follows:[69]

(i) The fastest one is the right running characteristic, which travels downstream with a velocity of $V_z + C$ (sum of the bulk velocity and speed of sound) and modifies temperature and pressure.
(ii) The second one is the entropy front, which travels with the bulk velocity of the fluid V_z.
(iii) The third one is the shock front, which travels with the velocity of the shock.

The shock front can be right or left traveling, and depending on the case, it can be faster or slower than the entropy front. In our case, the shock front was left traveling (in the relative frame of reference) and it was marching downstream in the absolute frame of reference with a speed of V_z – W, where W is the velocity of the flow seen by the moving shock. Each of these fronts can be clearly identified in Fig. 30(a).

As the shock front enters the blade-to-blade channel, the presence of strong adverse pressure gradients leads to boundary layer separation on both the pressure and suction sides [Fig. 30(b)]. Nonetheless, these separations remain confined, enabling the continued downstream progression of the shock wave [Figs. 30(c) and 30(d)]. Ultimately, the shock wave is released at the outlet, resulting in complete supersonic flow from the inlet to the outlet.

Furthermore, this simulation serves as evidence of the coarseness of the original Kantrowitz method, for which self-starting of this geometry was only attainable when the inlet Mach number exceeded 3.9.

In contrast, Fig. 31 presents the unsuccessful starting of the same blade row when the inlet Mach number was elevated to Mach 2.5. Since the inlet Mach number is above 2 (starting Mach number for the modified Kantrowitz), the shock enters inside the blade channel [Fig. 31(b)]. However, due to a combination of increased boundary layer separation and a lower inlet Mach number, flow choking occurs, resulting in a reversal of the shock motion [Figs. 31(c) and 31(d)]. Ultimately, the shock exits the blade channel and positions itself ahead of the row [Fig. 31(e)]. This second simulation demonstrates the importance of profile aerodynamics and boundary layer separation in the starting of a supersonic blade row.

The severity of boundary layer separation is strongly linked to the loading condition on the blade, which depends mainly on two factors: the solidity (c/g) and the profile shape. To study the influence of these two factors, four geometries (Table II) were considered with three distinct values for the solidity and two different profile shapes; unlike the "standard" geometry displayed in Fig. 31, the "impulse" shape is characterized by inlet and outlet geometric angles with opposite signs, resulting in a central region of the profile with zero inlet flow angle. If in the calculation of the area contraction A_{in}/A^* only the flow angles and the channel heights are accounted for (a common practice), the starting Mach number M_{start} for all four geometries is 3.9 for the original Kantrowitz method and 2 for the modified one. However, especially for the high-solidity cases, it is necessary to determine the throat area A^* more accurately. For this purpose, first, it is calculated the true geometric throat at the outlet of the blade row and then the area reduction due to the displacement thickness is estimated through the correlations proposed by Stratford and Beavers for compressible turbulent boundary layers.[70]

Furthermore, a completely automatized procedure was developed to calculate the corresponding starting limit with CFD simulations. The starting Mach number was found through a binary search

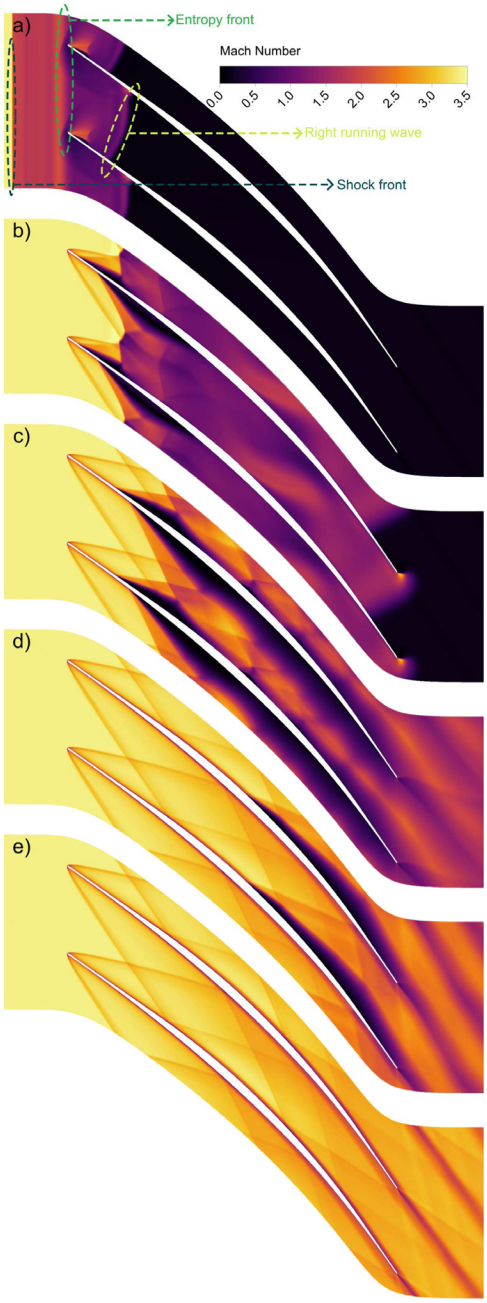

FIG. 30. Five instants extracted from the starting process of a supersonic blade with an inlet geometric angle of −35° and an outlet geometric angle of −56.4°. The inlet Mach number is raised with a single step from Mach 0.1 to 3.4. (The corresponding axial Mach numbers are 0.08 and 2.79.)

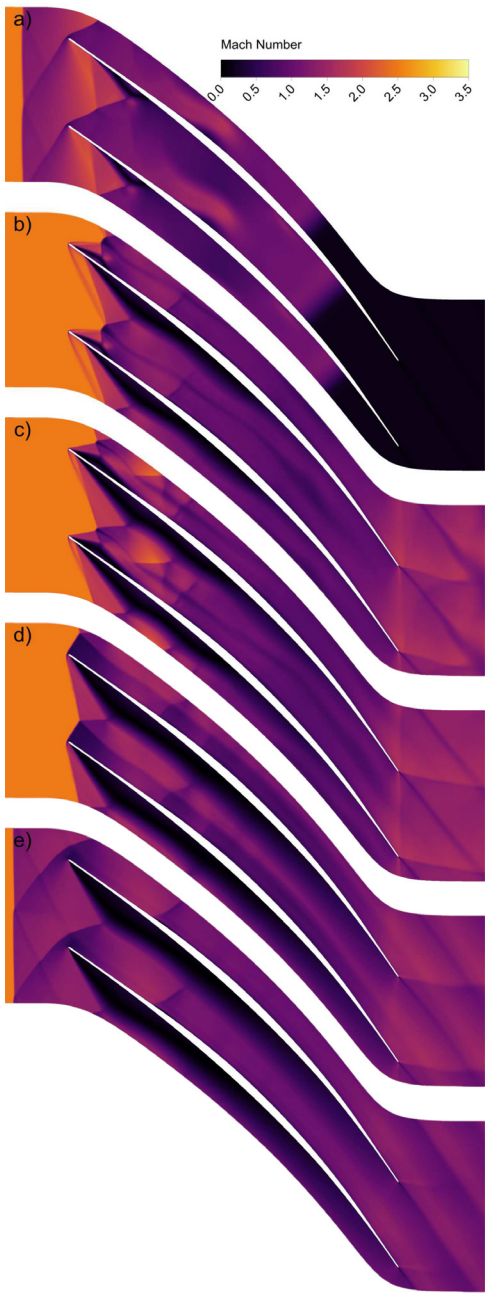

FIG. 31. Five instants extracted from the starting process of a supersonic blade with an inlet geometric angle of −35° and an outlet geometric angle of −56.4°. The inlet Mach number is raised with a single step from Mach 0.1 to 2.5. (The corresponding axial Mach numbers are 0.08 and 2.05.)

algorithm.[71] The search interval is halved at each iteration with one end satisfying the starting condition and the other not; the procedure is completed when the interval length is below 0.05 Mach. Since several time-accurate unsteady simulations are needed for each geometry, the calculation of each limit is computationally very expensive. A detailed description of the procedure is omitted for the sake of brevity, as it does not constitute novelty. The relationship between the starting Mach number and solidity does not exhibit a monotonic trend due to the interplay of two opposing factors; as the solidity is increased, the size of the boundary layer separation reduces because of

TABLE II. Geometries employed to evaluate the effect of the solidity and the profile shape on the starting Mach number.

Profile shape	β_{g-in}/ β_{g-out}	Solidity (c/g)	M_{start} modified Kantrowitz	M_{start} CFD
"Standard"	−35°/−56.4°	1.88	1.99	3.4
"Standard"	−35°/−56.4°	3.76	2.22	2.73
"Standard"	−35°/−56.4°	7.52	2.50	3.06
"Impulse"	−35°/56.4°	7.52	2.14	2.61

the lower loading on each blade, but at the same time, smaller boundary layers can have a larger relative weight in a smaller channel. Theoretically, it can be developed a procedure to determine the optimum solidity that minimizes the starting Mach number; however, the optimum solidity value is typically calculated to minimize losses in the started condition, which represents the majority of the machine's operating time.

Furthermore, the impulse shape demonstrates a lower starting Mach number compared to the standard shape at the same solidity. This difference can be attributed to the way the normal area changes from the inlet to the outlet. In the impulse shape, the geometric angle decreases, and the normal area increases in the first half of the blade. This increase in the normal area compensates for the reduction in area due to boundary layer separation, which ultimately facilitates the starting process.

The modified Kantrowitz criterion proposed in this study enhances the modeling of the phenomenon by identifying the correct shock structures generated ahead of a supersonic blade row, but it does not account for the intricate flow topology when the shock enters the blade-to-blade channel, leading to optimistic results. Conversely, the original Kantrowitz significantly overestimates the starting condition: The starting Mach number for all tested geometries was considerably lower than Mach 3.9 provided by the original methodology. While this conservative criterion has worked fine in the field of supersonic turbomachinery, it poses limitations for supersonic inlet turbines, which exhibit their highest efficiency close to the Kantrowitz starting limit;[23] an excessively conservative criterion eliminates the most efficient machines that do not actually suffer from starting issues. Unfortunately, addressing the inclusion of shock-induced boundary layer separation within a simple yet accurate model remains unresolved at the current stage.

To complete this section, Table III presents a comprehensive comparison between collective shock unstarting and Kantrowitz unstarting.

V. CONCLUSIONS

Avoiding unstarting phenomena is a necessary requirement for an efficient and safe operation of a supersonic inlet cascade. Although numerous publications exist on the starting of supersonic intakes, there is a significant gap in the understanding of these phenomena for supersonic blade rows. This paper aimed at bridging this knowledge gap by thoroughly investigating and modeling two distinct unstarting mechanisms observed in supersonic machines.

A novel unstarting mechanism was identified for supersonic cascades. Low inlet Mach numbers, high inlet geometric angles, and high incidence angles promote the coalescence of the leading-edge bow shock waves with the formation of a collective shock. The stability of this shock structure depends on the properties of the inlet channel: If the inlet channel is unstable, the collective shock propagates upstream and unstarts the supersonic channel. Furthermore, the phenomenon does not exhibit any hysteretic behavior since the formation and the disappearance of a collective shock occur at the same inlet Mach number. The characteristics of this additional unstarting mechanism were initially examined through detailed theoretical considerations and subsequently verified by CFD simulations.

A reduced order model was developed to predict the formation of a collective shock with limited data. The model accuracy was enhanced by re-evaluating Moeckel's methodology for predicting bow shock waves. To determine the asymptotic slope of the hyperbolic curve, an analogy was drawn between a bow shock and an oblique shock generated by a sharp corner. Additionally, a simple correlation was proposed to account for the increased thickness observed by the flow at large incidence angles. Model capabilities were verified against an extensive campaign of CFD simulations considering various inlet Mach numbers, inlet geometric angles, and incidence angles. The excellent agreement between model predictions and CFD results and the simplicity of the model itself enhance its practical value for the preliminary design of supersonic blade rows.

Moreover, the well-known Kantrowitz criterion for the self-starting of supersonic channels was reviewed and adjusted for its application to supersonic cascades. In the newly proposed formulation, shock structures consistent with the inlet conditions (weak or strong oblique shock waves) were considered in the calculation of the maximum contraction ratio. While the original Kantrowitz limit is excessively conservative, the modified criterion leads to optimistic results; in addition, both methods fail to account for the complex flow topology when the shock enters the blade channel. Finally, the effect of the blade solidity and the profile shape on the starting Mach number were

TABLE III. Comprehensive comparison between collective shock unstarting and Kantrowitz unstarting.

	Collective shock unstarting	Kantrowitz unstarting
Unstarting mechanism	Leading-edge bow shock wave coalescence generates a collective shock; if the inlet channel is unstable, the collective shock unstarts the supersonic channel.	During the starting of a supersonic blade row, a normal or an oblique shock wave appears at the entrance of the blade row if sonic conditions are reached before the throat in the converging channel.
Hysteretic behavior	No	Yes
Variables	M_{in}, β_{in}, i, g/th, γ, leading edge shape	M_{in}, α_{in}, blade aerodynamics
Simple and accurate model to predict the limit condition	Yes	No

studied, emphasizing the impact of shock-induced boundary layer separation on the starting process.

ACKNOWLEDGMENTS

The authors would like to thank Camilla Conti for providing us with the experimental data for the solver validation.

AUTHOR DECLARATIONS

Conflict of Interest

The authors have no conflicts to disclose.

Author Contributions

Noraiz Mushtaq: Conceptualization (equal); Data curation (equal); Formal analysis (lead); Methodology (equal); Software (lead); Validation (lead); Visualization (lead); Writing – original draft (lead); Writing – review & editing (equal). **Paolo Gaetani:** Conceptualization (equal); Data curation (equal); Methodology (equal); Project administration (lead); Supervision (lead); Writing – review & editing (equal).

DATA AVAILABILITY

The data that support the findings of this study are available from the corresponding author upon reasonable request.

NOMENCLATURE

a	ellipse semi-major axis (m)
ax	axial
A	area (m^2)
b	ellipse semi-minor axis (m)
c	chord (m)
corr	corrected
C	speed of sound (ms^{-1})
g	blade pitch (m) or geometric
i	incidence angle (deg)
in	inlet
k	model calibration constant (-)
M	Mach number (-)
n	normal
out	outlet
p	pressure (Pa)
t	time (s)
th	thickness (m)
V	velocity (ms^{-1})
W	velocity of the flow seen by the shock (ms^{-1})
X_0	foremost point of the shock (m)
z	axial direction
z_s'	shock position fluctuation (m)
α	flow angle (deg)
β	wave angle or profile geometric angle (deg)
γ	specific heat ratio (-)
θ	corner angle (deg)
μ	Mach angle (deg)
τ	time constant [Eq. (3)] (-)
ϕ_s	local inclination of the bow shock in the sonic point [Eq. (4)] (deg)
$\overline{()}$	Average value
$()'$	Fluctuation
$()^*$	Throat
CFD	computational fluid dynamics
MOC	method of characteristics
ORC	organic Rankine cycle
RANS	Reynolds averaged Navier–Stokes
RDC	rotating detonation combustor
RDE	rotating detonation engine
ROM	reduced order model

REFERENCES

[1]J. W. Kurzrock, "Experimental investigation of supersonic turbine performance," in Proceedings of the ASME 1989 International Gas Turbine and Aeroengine Congress and Exposition. Volume 1: Turbomachinery. Toronto, Ontario, Canada. June 4–8, 1989 Paper No: 89-GT-238, 1989.
[2]A. Stodola, *Dampf- Und Gasturbinen. Mit Einem Anhang Über Die Aussichten Der Wärmekraftmaschinen*, 5th ed. (Springer Berlin, Heidelberg, 1924), p. 1146.
[3]J. H. Keenan, "Reaction tests of turbine nozzles for supersonic velocities," Trans. Am. Soc. Mech. Eng. **71**, 773–779 (1949).
[4]C. H. Hauser, H. W. Plohr, and G. Sonder, "Study of flow conditions and deflection angle at exit of two-dimensional cascade of turbine rotor blades at critical and supercritical pressure ratios," Technical Report (NACA, 1950).
[5]H. Hausenblas, "Die Kennfelder der Turbinenteile von Gasturbinen," Forsch. Geb. Ingenieurwes. A **24**, 195–197 (1958).
[6]B. S. Stratford and G. E. Sansome, "The performance of supersonic turbine nozzles," Technical Report (Aeronautical Research Council R. M., 1959).
[7]B. S. Stratford and G. E. Sansome, "Theory and tunnel tests of rotor blades for supersonic turbines," Technical Report (Aeronautical Research Council R. M., 1960).
[8]L. J. Goldman, "Supersonic turbine design and performance," in Proceedings of the ASME 1972 International Gas Turbine and Fluids Engineering Conference and Products Show. ASME 1972 International Gas Turbine and Fluids Engineering Conference and Products Show. San Francisco, California, USA, March 26–30, 1972 (1972).
[9]K. Kawatsu, N. Tani, M. Shimagaki, M. Uchiumi, N. Yamanishi, K. Mitsuhashi, and T. Mizuno, "Multi objective optimization of a supersonic axial turbine blade row shape for rocket engine turbopump," AIAA Paper No. 2011-5784, 2011.
[10]D. J. Dorney, L. W. Griffin, and F. W. Huber, "A study of the effects of tip clearance in a supersonic turbine," J. Turbomach. **122**, 674–683 (2000).
[11]A. S. Leyzerovich, "Steam turbines for modern Fossil-Fuel power plants," in *Steam Turbines for Modern Fossil-Fuel Power Plants* (River Publishers, 2008), pp. i–xiv.
[12]S. Senoo, "Development of design method for supersonic turbine aerofoils near the tip of long blades in steam turbines: Part 1-Overall configuration," in ASME Turbo Expo 2012: Turbine Technical Conference and Exposition (2012).
[13]P. Wolański, "Detonative propulsion," Proc. Combust. Inst. **34**, 125–158 (2013).
[14]S. M. Jones and D. E. Paxson, "Potential benefits to commercial propulsion systems from pressure gain combustion," AIAA Paper No. 2013-3623, 2013.
[15]E. Wintenberger and J. E. Shepherd, "Thermodynamic cycle analysis for propagating detonations," J. Propul. Power **22**, 694–698 (2006).
[16]S. M. Frolov, A. V. Dubrovskii, and V. S. Ivanov, "Three-dimensional numerical simulation of operation process in rotating detonation engine," Prog. Propul. Phys. **4**, 467–488 (2013).
[17]J. Sousa, G. Paniagua, and E. Collado Morata, "Thermodynamic analysis of a gas turbine engine with a rotating detonation combustor," Appl. Energy **195**, 247–256 (2017).
[18]S. Claflin, S. Sonwane, E. Lynch, and J. Stout, "Recent advances in power cycles using rotating detonation engines with subcritical and supercritical CO_2," in

4th International Symposium - Supercritical CO2 Power Cycles, *Pittsburgh* (2014).
[19]G. Paniagua, M. C. Iorio, N. Vinha, and J. Sousa, "Design and analysis of pioneering high supersonic axial turbines," Int. J. Mech. Sci. **89**, 65–77 (2014).
[20]J. Sousa and G. Paniagua, "Entropy minimization design approach of supersonic internal passages," Entropy **17**, 5593 (2015).
[21]Z. Liu, J. Braun, and G. Paniagua, "Characterization of a supersonic turbine downstream of a rotating detonation combustor," J. Eng. Gas Turbines Power **141**, 1–13 (2019).
[22]N. Mushtaq, G. Colella, and P. Gaetani, "Design and parametric analysis of a supersonic turbine for rotating detonation engine applications," Int. J. Turbomach., Propul. Power **7**, 1 (2022).
[23]N. Mushtaq, G. Persico, and P. Gaetani, "The role of endwall shape optimization in the design of supersonic turbines for rotating detonation engines," J. Turbomach. **145**, 081015 (2023).
[24]J. Sousa, G. Paniagua, and J. Saavedra, "Aerodynamic response of internal passages to pulsating inlet supersonic conditions," Comput. Fluids **149**, 31 (2017).
[25]J. Braun, Z. Liu, D. Cuadrado, V. Andreoli, G. Paniagua, J. Saavedra, V. Athmanathan, and T. R. Meyer, "Characterization of an integrated nozzle and supersonic axial turbine with a rotating detonation combustor," AIAA Paper No. 2019-3873, 2019, pp. 1–11.
[26]D. Shen, M. Cheng, K. Wu, Z. Sheng, and J. Wang, "Effects of supersonic nozzle guide vanes on the performance and flow structures of a rotating detonation combustor," Acta Astronaut. **193**, 90–99 (2022).
[27]L. Su, F. Wen, C. Wan, Z. Li, J. Han, S. Wang, and Z. Wang, "Large-eddy simulation study of rotating detonation supersonic turbine nozzle generated by the method of characteristics under oscillating incoming flow," Phys. Fluids **34**, 116119 (2022).
[28]E. Bach, C. O. Paschereit, P. Stathopoulos, and M. D. Bohon, "Rotating detonation wave direction and the influence of nozzle guide vane inclination," AIAA J. **59**, 5276–5287 (2021).
[29]F. Lozano and G. Paniagua, "Airfoil leading edge blowing to control bow shock waves," Sci. Rep. **10**, 21922 (2020).
[30]F. Falempin and B. Le Naour, "R&T effort on pulsed and continuous detonation wave engines," AIAA Paper No. 2009-7284, 2009.
[31]P. Stathopoulos, "Comprehensive thermodynamic analysis of the Humphrey cycle for gas turbines with pressure gain combustion," Energies **11**, 3521 (2018).
[32]P. Colonna, E. Casati, C. Trapp, T. Mathijssen, J. Larjola, T. Turunen-Saaresti, and A. Uusitalo, "Organic Rankine cycle power systems: From the concept to current technology, applications, and an outlook to the future," J. Eng. Gas Turbines Power **137**, 100801 (2015).
[33]G. Persico and M. Pini, *8 - Fluid Dynamic Design of Organic Rankine Cycle Turbines* (Woodhead Publishing, 2017), pp. 253–297.
[34]E. A. Bufi and P. Cinnella, "Preliminary design method for dense-gas supersonic axial turbine stages," J. Eng. Gas Turbines Power **140**, 112605 (2018).
[35]P. Colonna, J. Harinck, S. Rebay, and A. Guardone, "Real-gas effects in organic Rankine cycle turbine nozzles," J. Propul. Power **24**, 282–294 (2008).
[36]A. Romei, D. Vimercati, G. Persico, and A. Guardone, "Non-ideal compressible flows in supersonic turbine cascades," J. Fluid Mech. **882**, A12 (2020).
[37]J. Sousa, G. Paniagua, and E. Collado-Morata, "Analysis of the aerodynamic losses in a supersonic turbine," in *American Society of Mechanical Engineers, Power Division (Publication) Power* (ASME, 2017), Vol. 1, pp. 1–7.
[38]H. Starken, Z. Yongxing, and H.-A. Schreiber, "Mass flow limitation of supersonic blade rows due to leading edge blockage," in Proceedings of the ASME 1984 International Gas Turbine Conference and Exhibit. Volume 1: Turbomachinery. Amsterdam, The Netherlands. June 4–7, 1984 (1984).
[39]H.-J. Lichtfuss and H. Starken, "Supersonic cascade flow," Prog. Aerosp. Sci. **15**, 37–149 (1974).
[40]W. H. Heiser and D. T. Pratt, *AIAA Education Series* (American Institute of Aeronautics and Astronautics, 1994).
[41]A. Kantrowitz and C. Donaldson, "Preliminary investigation of supersonic diffusers," NACA Wartime Reports (1945).
[42]J. Chang, N. Li, K. Xu, W. Bao, and D. Yu, "Recent research progress on unstart mechanism, detection and control of hypersonic inlet," Prog. Aerosp. Sci. **89**, 1–22 (2017).
[43]A. Kantrowitz, "The supersonic axial-flow compressor," Technical Report (1946).
[44]L. J. Goldman and M. R. Vanco, "Computer program for design of two-dimensional sharp-edged-throat supersonic nozzle with boundary-layer correction," NASA (1971).
[45]ANSYS. "ANSYS CFX-solver theory guide," Technical Report (ANSYS Inc., 2021).
[46]M. C. Druguet and D. E. Zeitoun, "Influence of numerical and viscous dissipation on shock wave reflections in supersonic steady flows," Comput. Fluids **32**, 515 (2003).
[47]T. BARTH and D. JESPERSEN, "The design and application of upwind schemes on unstructured meshes," in *27th Aerospace Sciences Meeting, Aerospace Sciences Meetings* (American Institute of Aeronautics and Astronautics, 1989).
[48]ANSYS. "ANSYS TurboGrid reference guide," Technical Report (ANSYS, Inc., 2021).
[49]I. B. Celik, U. Ghia, P. J. Roache, C. J. Freitas, H. Coleman, and P. E. Raad, "Procedure for estimation and reporting of uncertainty due to discretization in CFD applications," J. Fluids Eng., Trans. ASME **130**, 780011–780014 (2008).
[50]G. A. Sod, "A numerical study of a converging cylindrical shock," J. Fluid Mech. **83**, 785 (1977).
[51]G. Settles and L. Dodson, "Hypersonic shock/boundary-layer interaction database: New and corrected data," Pennsylvania State University Report (1994).
[52]C. C. Conti, A. Fusetti, A. Spinelli, and A. Guardone, "Shock loss measurements in non-ideal supersonic flows of organic vapors," Exp. Fluids **63**, 117 (2022).
[53]G. S. Settles and L. J. Dodson, "Hypersonic shock/boundary-layer interaction database," AIAA Paper No. 91-1763, 1991.
[54]V. M. Boiko, K. V. Klinkov, and S. V. Poplavskii, "Collective bow shock ahead of a transverse system of spheres in a supersonic flow behind a moving shock wave," Fluid Dyn. **39**, 330–338 (2004).
[55]S. J. Laurence, R. Deiterding, and G. Hornung, "Proximal bodies in hypersonic flow," J. Fluid Mech. **590**, 209–237 (2007).
[56]J. Délery and J. P. Dussauge, "Some physical aspects of shock wave/boundary layer interactions," Shock Waves **19**, 453 (2009).
[57]J. D. Anderson, *Modern Compressible Flow: With Historical Perspective, Aeronautical and Aerospace Engineering Series* (McGraw-Hill Education, 2003).
[58]N. Mushtaq and P. Gaetani, "The effect of upstream unsteadiness on the unstarting of a supersonic inlet turbine," in *ASME Turbo Expo 2023* (ASME, 2023), GT2023–103883.
[59]W. E. Moeckel, "Approximate method for predicting form and location of detached shock waves ahead of plane or axially symmetric bodies," NASA TN (1921), Vol. 211, p. 130.
[60]J. Braun, G. Paniagua, and D. Ferguson, "Aero-thermal characterization of accelerating and diffusing passages downstream of rotating detonation combustors," in *ASME Turbo Expo 2021* (ASME, 2021), GT2021–59111.
[61]F. E. C. Culick and T. Rogers, "The response of normal shocks in diffusers," AIAA J. **21**, 1382–1390 (1983).
[62]J. M. Burgers, "Aerodynamics. On the transmission of sound waves through a shock wave BT—Selected Papers of J. M. Burgers," (Springer Netherlands, Dordrecht, 1995), pp. 478–486.
[63]A. Kantrowitz, "The formation and stability of normal shock waves in channel flows," Technical Report (NACA, 1947).
[64]H. G. Hurrell, "Analysis of shock motion in ducts during disturbances in downstream pressure," Technical Report (NACA, 1957).
[65]H.-G. Pagendarm and B. Seitz, "An algorithm for detection and visualization of discontinuities in scientific data fields applied to flow data with shock waves," in III. Eurographics Workshop in Visualization in Scientific Computing, Viareggio, Italy, 27–29 April, 1992.

[66]E. S. Love, "A reexamination of the use of simple concepts for predicting the shape and location of detached shock waves," Technical Report. (NACA, 1957).
[67]X. Veillard, R. Tahir, E. Timofeev, and S. Molder, "Limiting contractions for starting simple ramp-type scramjet intakes with overboard spillage," J. Propul. Power **24**, 1042–1049 (2008).
[68]A. K. Flock and A. Gülhan, "Modified Kantrowitz starting criteria for mixed compression supersonic intakes," AIAA J. **57**, 2011–2016 (2019).
[69]A. H. Shapiro, *Dynamic and Thermodynamics of Compressible Fluid Flow* (John Wiley Sons Inc, 1953), Vol. I, p. 647.
[70]B. S. Stratford and G. S. Beavers, "The calculation of the compressible turbulent boundary layer in an arbitrary pressure gradient—A correlation of certain previous methods," Aeronautical Research Council Reports (1961).
[71]D. E. Knuth, *The Art of Computer Programming* (Pearson Education, 1997), Vol. 3.